

1950

# The uranium-carbon system: the structure of dimethylberyllium and its bearing on chemical valence

Adolph Isaac Snow  
*Iowa State College*

Follow this and additional works at: <https://lib.dr.iastate.edu/rtd>

 Part of the [Physical Chemistry Commons](#)

## Recommended Citation

Snow, Adolph Isaac, "The uranium-carbon system: the structure of dimethylberyllium and its bearing on chemical valence" (1950).  
*Retrospective Theses and Dissertations*. 15180.  
<https://lib.dr.iastate.edu/rtd/15180>

This Dissertation is brought to you for free and open access by the Iowa State University Capstones, Theses and Dissertations at Iowa State University Digital Repository. It has been accepted for inclusion in Retrospective Theses and Dissertations by an authorized administrator of Iowa State University Digital Repository. For more information, please contact [digirep@iastate.edu](mailto:digirep@iastate.edu).

# NOTE TO USERS

This reproduction is the best copy available.

**UMI**<sup>®</sup>



UNCLASSIFIED

Title: The Uranium-Carbon System; The Structure of Dimethylberyllium  
and Its Bearing on Chemical Valence

Author: Adolph Isaac Snow

(Official certification of the classification shown is filed in the  
Ames Laboratory Document Library)

Signature was redacted for privacy.

W. E. Dreeszen

Secretary to Declassification  
Committee

UNCLASSIFIED



**THE URANIUM-CARBON SYSTEM; THE STRUCTURE OF DIMETHYLBERYLLIUM  
AND ITS BEARING ON CHEMICAL VALENCE**

by

**Adolph Isaac Snow**

A Dissertation Submitted to the  
Graduate Faculty in Partial Fulfillment of  
The Requirements for the Degree of  
**DOCTOR OF PHILOSOPHY**

**Major Subject: Physical Chemistry**

**Approved:**

Signature was redacted for privacy.

**In Charge of Major Work**

Signature was redacted for privacy.

**Head of Major Department**

Signature was redacted for privacy.

**Dean of Graduate College**

**Iowa State College**

**1950**

UMI Number: DP12965

### INFORMATION TO USERS

The quality of this reproduction is dependent upon the quality of the copy submitted. Broken or indistinct print, colored or poor quality illustrations and photographs, print bleed-through, substandard margins, and improper alignment can adversely affect reproduction.

In the unlikely event that the author did not send a complete manuscript and there are missing pages, these will be noted. Also, if unauthorized copyright material had to be removed, a note will indicate the deletion.

**UMI**<sup>®</sup>

---

UMI Microform DP12965

Copyright 2005 by ProQuest Information and Learning Company.

All rights reserved. This microform edition is protected against unauthorized copying under Title 17, United States Code.

ProQuest Information and Learning Company  
300 North Zeeb Road  
P.O. Box 1346  
Ann Arbor, MI 48106-1346

TABLE OF CONTENTS

INTRODUCTION . . . . .	1
THE URANIUM-CARBON SYSTEM . . . . .	3
I. Introduction . . . . .	3
II. Historical Background . . . . .	3
III. Materials and Apparatus . . . . .	4
IV. Constitutional Diagram . . . . .	8
A. Uranium Solid Transformations and Solidus from 0-4.8 wt.% Carbon . . . . .	8
B. Identification of UC . . . . .	10
C. Determination of Liquidus Line from 0-4.8 wt.% Carbon . . . . .	11
D. Identification of $U_2C_3$ and $UC_2$ . . . . .	14
E. Melting Points of UC, $U_2C_3$ , and $UC_2$ . . . . .	17
F. Equilibrium Relationships among UC, $U_2C_3$ , and $UC_2$ . . . . .	18
V. Hardness of U-C Alloys from 0-4.8 wt.% Carbon . . . . .	21
VI. X-Ray Study of the Uranium-Carbon System . . . . .	21
A. Uranium Monocarbide, UC . . . . .	21
B. Nitrogen and Oxygen Contamination of UC . . . . .	22
C. Uranium Sesquicarbide, $U_2C_3$ . . . . .	24
D. Uranium Dicarbide, $UC_2$ . . . . .	25
VII. Polishing and Etching . . . . .	27
THE STRUCTURE OF DIMETHYLBERYLLIUM AND ITS BEARING ON CHEMICAL VALENCE . . . . .	40
I. Introduction and Historical Background . . . . .	40
II. Preparation of the Compound . . . . .	49
III. Identification of Dimethylberyllium . . . . .	57
IV. Determination of the Structure . . . . .	59
A. X-Ray Equipment . . . . .	59
B. Measurement of Intensities . . . . .	59
C. Laue Symmetry . . . . .	61



TABLE OF CONTENTS (continued)

D. Determination of Lattice Constants . . . . .	61
E. Determination of the Density of Dimethylberyllium . . . . .	61
F. Determination of the Possible Space Groups .	62
G. Determination of Parameters . . . . .	64
H. Temperature Factor and Parameter Refinement	69
I. Effect of the Hydrogen Atoms . . . . .	73
J. Structure Factor Agreement . . . . .	76
K. Discussion of the Structure . . . . .	81
METALLIC VALENCES . . . . .	91
SUMMARY . . . . .	100
I. The Uranium-Carbon System . . . . .	100
II. The Structure of Dimethylberyllium . . . . .	101
III. Metallic Valences . . . . .	102
LITERATURE CITED . . . . .	104
ACKNOWLEDGMENTS . . . . .	109

## INTRODUCTION

The topics discussed in this thesis and the order in which they are arranged rather accurately reflect the trend of the author's interests with time.

Because of the work on the phase diagram described here and also experimental work on other alloy systems and some problems in the casting of metals and metal fabrication the author became interested in the bonding of solids. This led to the use of X-ray diffraction which is one of the most powerful tools for investigating the structure of solids.

The determination of the structure of dimethylberyllium by means of X-ray diffraction is of theoretical value since it is another link in the chain of evidence concerning electron deficient compounds and, in fact, is a striking confirmation of the theory, first proposed by Dr. R. E. Rundle that metals with more low energy orbitals than valence electrons should form electron deficient compounds when combined with groups containing no unshared electron pairs. The theory which explains the bonding in dimethylberyllium may also be successfully applied to explain the bonding in various intermetallic compounds and, in fact, has been so applied by Rundle and Pauling.

Determination of crystal structures by means of X-ray diffraction led naturally to interest in the theory of intermetallic bonding and, in particular, metallic valences which are discussed in the last section of this thesis.

Thus, it may be seen that the apparently unrelated sections of this thesis are bound together by the author's interests which have progressed from the strictly experimental to the somewhat theoretical.

## THE URANIUM-CARBON SYSTEM

### I. Introduction

The need for a complete study of the uranium-carbon system arose from: (1) experiments at Iowa State College (under contract with the Manhattan District, U. S. Corps of Engineers) which showed that uranium could be cast in graphite without excessive carbon contamination, and (2) requests for cast forms of uranium carbide for experimental pile studies.

Chemical, thermal, metallographic, and X-ray methods of analysis have been employed in this study which covers the entire binary system.

### II. Historical Background

Perhaps the earliest attempt to make uranium carbides was that of Moissan (1) (1896) who reported the preparation of a metallic, crystalline material by reaction between  $U_3O_8$  and carbon in an electric furnace to give a compound which he supposed to be  $U_2C_3$ . Although his analyses showed a carbon content slightly higher than the theoretical value, he thought that  $U_2C_3$  was a definite compound and also that it was the highest carbon compound possible in this system.

In 1911 Lebeau (2) reported the preparation of  $UC_2$  which he assumed to be the same material as Moissan's  $U_2C_3$ . He explained the difference in formula by supposed errors existing in the analysis method used by Moissan.

Also in 1911, Ruff and Heinzelmann (3) reported the preparation of a compound analyzing closely to the theoretical composition of  $UC_2$ . They reported the melting point to be  $2425^{\circ}C$ .

G. Hägg (4) in 1931 determined the crystal structure of a  $UC_2$  sample, prepared by Arnfelt, by means of X-ray diffraction studies.

Polushkin (5) (1921) while investigating iron-uranium alloys, produced by reducing mixtures of  $U_3O_8$  and steel turnings with petroleum coke, found that uranium carbides were present in the iron. These carbides were assumed to be UC and  $U_2C_3$ .

With the exception of Hagg none of these investigators had any definite proof of the existence of their "compounds". In each case the composition was deduced from chemical analysis with slight additional proof that such a compound actually existed.

### III. Materials and Apparatus

The uranium used in this investigation was metal produced at Ames for Manhattan project purposes. Two forms were used (1) metal recast into graphite molds containing carbon as the main impurity and (2) "biscuit metal" which is unrecast and contains some impurities.

When this investigation began an occasional production billet would contain a relatively large amount of iron ( $> 300$  ppm). Use of this material in preparing carbon alloys caused some misinterpretation of

microstructures at first but this impurity did not seem to affect thermal breaks appreciably. Eventually anomalies in microstructures were traced to iron content and the effect of iron could be compensated for in interpreting microstructures. (6,7,8) Other impurities present were oxides and nitrides due to the great affinity of the metal for these elements. Although they could not be eliminated completely, their effect was lessened by preparing all samples in vacuum.

The carbon in the samples was added in several ways. Usually the uranium was heated in crucibles made of Acheson AGR and AGOT graphite and the carbon was dissolved from the walls of the crucible. Although the AGOT graphite is purer than the AGR grade in some respects, microstructures obtained from castings in these crucibles were identical. (9) When the carbon was added to the samples as a powder, Acheson AGR, AGOT and grade #38 graphite were used.

For alloys in which no change in carbon content on heating was desired  $\text{BeO}$ ,  $\text{ZrO}_2$ , and  $\text{ThO}_2$  crucibles were tried. Of these,  $\text{BeO}$  was found to be the most satisfactory because of its unusual resistance to cracking from thermal shock and the fact that it does not react with carbon appreciably below  $2050^\circ\text{C}$ .  $\text{ThO}_2$  and  $\text{ZrO}_2$  are much more subject to cracking and react with graphite at  $1750\text{-}1800^\circ\text{C}$ . These crucibles were made by the Ames ceramic section and by the author either by slip casting or tamping.

An induction furnace was used for preparing the samples and for some thermal analyses. The heater, consisting of a graphite crucible

with a tight fitting cover and a long chimney, was well insulated from the quartz vacuum jacket by an inch and a half layer of Norblack, a special grade of lamp black. Temperatures estimated as high as 3000°C were attained with this set-up.

Temperature measurements were made by means of a Leeds and Northrup optical pyrometer, and chromel-alumel and platinum-platinum rhodium thermocouples. The long chimneys used on the heater crucibles insured reasonably good black body conditions for the optical pyrometer readings. Thermal data were plotted to give the inverse rate type of cooling curve.

Some measurements of the uranium solid transformation temperatures were made with a Leeds and Northrup differential transformation apparatus in which a platinum resistance furnace was used to heat the sample and a nickel crucible served as the neutral body. (15) In this device sample temperature is plotted as the ordinate and difference between sample and crucible temperature as the abscissa. This method is a sensitive one for the location of small heat effects.

Alloys were prepared in several ways.

1. By solution from the casting crucible. (10)

The metal was cast into a graphite crucible and held at some fixed temperature for a period of time long enough to allow the molten metal to dissolve carbon off the crucible walls. Fairly uniform alloys were obtained in most melts by this method. In all cases adjacent areas were used for carbon analysis and metallographic study.

2. By sintering powdered uranium and carbon compacts. (11)

Powdered uranium metal, made by decomposing uranium hydride, (12) was intimately mixed with powdered graphite and compacted under pressure. Due to the extremely pyrophoric nature of powdered uranium all manipulations had to be performed in a vacuum or in an inert atmosphere (usually  $\text{CO}_2$ ). After they were pressed the briquettes could be handled for a short time in air. These samples were sintered in BeO crucibles for alloys melting below  $2000^\circ\text{C}$ . Alloys melting above  $2000^\circ\text{C}$  were placed on a uranium carbide block and heated to the desired temperature. This was an extremely effective way of preparing some of the samples since there was no reaction of the sample with its support.

3. Large amounts of  $\text{U}_2\text{C}_3$  and  $\text{UC}_2$  were prepared by Daane by heating  $\text{UO}_2$  and carbon in graphite crucibles to approximately  $2400^\circ\text{C}$ . (13) In order to produce  $\text{U}_2\text{C}_3$  it was necessary to add  $\text{UO}_2$  to the melt while the reaction between carbon and the dioxide was occurring. If this procedure was not followed, only  $\text{UC}_2$  resulted.

4. Other methods tried were: (14)

- a. heating uranium turnings with powdered carbon in graphite crucibles
- b. heating uranium turnings with powdered  $\text{U}_2\text{C}_3$  or  $\text{UC}_2$
- c. heating pressed blocks of powdered uranium mixed with powdered UC

All of these methods yielded identical results when the samples were allowed to come to equilibrium.

It was necessary to clean the uranium metal before casting since uncleaned samples always had an oxide or carbide crust which did not



allow the samples to flow. The most effective cleaning method was a soak in 1-1 nitric acid, which usually removed most of the surface scale. Small amounts of fused  $MgF_2$  or  $CaF_2$  slag, which sometimes remained after the acid soak, were easily ground off.

#### IV. Constitutional Diagram

##### A. Uranium Solid Transformations and Solidus from 0-4.8 wt% Carbon

All attempts to obtain the liquidus line of this system by means of thermocouples failed so that only the solidus up to 4.8 wt% and the uranium solid transformation temperatures could be determined by ordinary cooling curve techniques. Sample data are given in Table 1. Blank spaces indicate undetermined data. Some of these data were obtained by Dr. J. H. Carter.

The microstructures and X-ray photographs suggest that the last liquid freezing in these alloys is pure uranium. The Battelle laboratory has presented evidence for a small amount of solubility of UC in gamma uranium which may be evidence for a peritectic reaction in the region around 0.1% carbon (16).

The values for the gamma-beta solid transformation, given in Table 1, show no significant variation from the 0.03% carbon sample to the higher carbon alloys and, considering the limits of error of the determination, are in agreement with the reported value for pure uranium.

The beta-alpha values are slightly lower than the reported value of  $662^{\circ}C$ , (17) but since they fall within the range of values reported

Table 1 (15)

Solidification and Transformation Temperatures of Uranium-Carbon Alloys

% Carbon	$\gamma$ - $\beta$ Transformation			$\beta$ - $\alpha$ Transformation	
	Solidification Temperat.	L + N differen- tial recorder	Inverse Rate Cooling Curve	L + N differen- tial recorder	Inverse Rate Cooling Curve
0.03	1134°C	775°C	759°C	645°C	640°C
0.091	----	774	---	649	---
0.11	1130	782	775	643	645
0.14	----	787	---	649	---
0.17	----	780	---	643	---
0.39	----	785	---	652	---
0.42	1130	788	770	643	640
0.47	1134	777	774	648	650
0.63	----	793	---	635	---
0.77	1128	770	768	625	630
1.20	1123	777	768	636	640
1.50	1123	766	760	633	635

All temperatures  $\pm 15^\circ\text{C}$

by Manhattan project investigators for pure uranium, the effect of carbon on this transformation is probably very small.

The microstructures of these alloys show an increasing amount of a dendritic phase which forms in lakes as the carbon content increases. (See Figures 1-9) The fact that carbide inclusions are noted in concentrations down to 0.007 wt% carbon shows that an eutectic, if such exists, must lie close to zero per cent carbon.

#### B. Identification of UC

The following methods were used by Carter, Tevebaugh, and the author to separate the dendritic phase observed in low carbon samples.

1. Solution of the excess metal in HCl. (18) This method gave a considerable amount of uranium oxide which was removed by gravity separation.

2. Solution of the excess metal in an HCl-H<sub>2</sub>O<sub>2</sub> mixture which produced considerably less oxide than the above method. A 3 molar HCl solution was used and enough H<sub>2</sub>O<sub>2</sub> was added to prevent precipitation of uranium oxides.

3. Conversion of the excess metal to hydride and sifting out the inclusions on a 400 mesh sieve.

The separated material had the same appearance as the inclusions present in the alloys. Figure 10 shows some of the separated dendrites, a few of which have retained their original shape.

A typical analysis of the material obtained from each of the three

methods of separation showed:

% U	94.90
% C	4.70
% N	0.016
% O	0.384 (by difference)

Spectrographic examination showed only trace quantities of other metallic substances so that the oxygen content could be assumed by difference with a reasonable degree of accuracy, and, assuming the oxygen to be present as  $UO_2$  and the nitrogen as UN, this leaves a U:C ratio of 1:1.01.

X-ray photograms of these inclusions showed that they were cubic crystals, different from any of the higher carbides. (See X-ray section).

A sample containing 4.8 wt% carbon was carefully prepared by briquetting a mixture of powdered uranium and carbon and heating this to 2000°C on a  $U_2C_3$  block. The microstructure of this sample showed one phase which etched the same as the dendritic inclusions in the lower carbon alloys, and X-ray photograms were found to agree perfectly with those of the separated dendrites.

The melting point of UC is approximately 2350-2400°C (see section IVE).

#### C. Determination of Liquidus Line from 0-4.8 wt% Carbon

Since it was impossible to obtain any indications of a liquidus break in the 0-4.8 wt% carbon samples, it was necessary to resort to other methods than cooling curves to determine the liquidus (19).

Thermal data taken with an optical pyrometer sighted on a closed end refractory tube immersed in the metal gave a good value for the solidus but no reliable indications of the liquidus.

A method used in an attempt to locate the liquidus line was metallographic examination of pressed and sintered briquettes of mixtures of powdered UC and U which had been heated to definite temperatures for a long enough time to obtain equilibrium conditions. (20) The monocarbide which had dissolved in the molten metal was precipitated in the form of dendrites or lakes. As the liquidus line was approached the dendrites became larger. In the specimens in which the UC had not completely dissolved two areas were visible; (1) an upper zone consisting of undissolved UC particles which had floated to the top of the specimen (Figure 11) and (2) a lower area consisting of UC dendrites in a metal matrix (Figure 12). In those samples in which solution was complete only large dendrites in a uranium matrix were observed (Figure 13). By this method an 0.41 wt% carbon alloy was found to be completely liquid at 1950°C, but not at 1700°C.

Though this procedure could have been refined to give narrower temperature ranges and, therefore, more precise results, a more feasible method was devised which was used to determine the liquidus values given in Figure 27.

Cylinders of uranium metal were heated in graphite crucibles at definite temperatures for a long enough time to allow a carbide layer to form on the interface between the molten metal and the crucible and

for equilibrium conditions to exist between the metal and the carbide layer. (19)

It had been noted that when uranium was heated in graphite crucibles for long periods of time a crust formed on the graphite from which the metal could easily be separated. The microstructure of a horizontal cross section of such a sample showed that the outside crust contained the high melting carbides with UC forming a layer inside of this, and the center consisted of a uranium metal matrix containing UC dendrites. The distribution of phases may be explained in the following manner: When the uranium is first melted in the graphite crucible, it dissolves carbon from the walls and becomes saturated with UC. Additional uranium carbide that is formed builds up on the crucible wall and this reacts with the crucible to form higher carbides which in turn build up on the walls of the crucible. If this process were allowed to continue for a long enough period of time the entire sample would consist of the highest carbide possible, but heating is not carried out long enough to allow this to occur. UC and the higher carbides are solid at the temperatures used in this determination, and only the uranium is molten. This molten uranium reacts with the UC wall until, at equilibrium at a definite temperature, it becomes saturated with UC. Since the liquidus line represents the solubility of UC in molten uranium at various temperatures, the position of the liquidus may be obtained by plotting the carbon content of the central portion (uranium metal) of each of the heated cylinders against its equilibrium temperature.

Samples for chemical analysis were taken from the center of each alloy, and, to avoid errors due to segregation of the UC on cooling, three or four vertical sections were analyzed from each sample.

The cylinders, 3 cm in diameter and 2.2 cm tall, were heated in an induction furnace and held at the desired temperature ( $\pm 50^{\circ}\text{C}$ ) for periods of time ranging from two to two and one-half hours. Samples heated for longer periods of time showed that equilibrium conditions were reached in two hours. Figure 27, shows the liquidus as determined by this method. Each short vertical line represents the degree of accuracy of the temperature measurements. This range could be improved by use of a heat source capable of better control than an induction furnace.

The steepness of the curve up to  $1800^{\circ}\text{C}$  explains why casting of uranium in graphite crucibles has been successful. The usual casting temperature for large scale production of uranium is about  $1300^{\circ}\text{C}$  and this temperature should result in a maximum carbon content of less than 0.1 wt% carbon according to Figure 27. In ordinary casting procedures, equilibrium conditions are never approached because of the size of the charge and the short time approached because of the size of the charge and the short time during which the uranium is molten. This method gives finished metal with a carbon content of about 300 ppm.

#### D. Identification of $\text{U}_2\text{C}_3$ and $\text{UC}_2$

$\text{UC}_2$  had been studied by X-ray methods and confirmed as a compound before the project began. X-ray work at Ames confirmed earlier results.

For details see the X-ray section of this report.

Under the microscope alloys of composition close to that of  $U_2C_3$  appear as a two phase area arranged in a striking Widmanstatten pattern (Figures 15 and 16). When examined by X-ray diffraction the phases are shown to be UC and  $UC_2$ . At 7.03 wt% carbon, the formula value for  $U_2C_3$ , the macrocrystals are perfectly cubic, but when the carbon composition is just a little higher or lower than this value, the cubes are distorted although the microstructure is practically unchanged. Since the Widmanstatten structure is indicative of a decomposition of a one phase area, alloys of composition close to that of  $U_2C_3$  were quenched from various temperatures in an effort to obtain a one phase area but in each case the typical Widmanstatten structure resulted (Figures 16 and 17). Even quenching the molten  $U_2C_3$  in molten lead did not change the microstructure. (21)

Because of the Widmanstatten structure appearing within the grains at this composition, it is probable that this carbide consists of one solid phase at some high temperature. Perhaps it is a cubic compound at 7.03% carbon but off to each side of this value it dissolves some UC or  $UC_2$  and so distorts its structure. An alternative explanation is that a solid solution of UC and  $UC_2$  exists at high temperatures which decomposes to give the microstructures observed. In the phase diagram presented in this paper, the compound is suggested as a stable phase at high temperature with some solubility of UC and  $UC_2$  in it. See the X-ray section for a further discussion of the existence of  $U_2C_3$  as a definite compound at high temperature.



Recently Mallett, Gerds, and Vaughan at the Battelle Memorial Institute (30) have unsuccessfully attempted to obtain a one phase microstructure at compositions in the vicinity of that of  $U_2C_3$  by annealing for "reasonable" periods of time in the temperature range 1250-1800°C. They have found, however, that if a sample of  $U_2C_3$  is cold worked and then annealed at 1600°C. a monophasic microstructure is obtained. The most complete conversion to one phase is obtained by heating a sample at 2000°C. for  $\frac{1}{2}$  hour in a vacuum and then cooling to 1600°C. The sample is "then held at 1600 degrees for two hours in a vacuum, being jostled about in the crucible, at intervals by means of a remotely controlled tungsten rod during the 1600°C. heat treatment." No sample has been converted wholly to one phase. The maximum conversion has been 90%. Surprisingly it was found that even the small amount of cold work put into a sample by removing it from a furnace and placing it in a glass vial on a work bench for a half hour was enough to cause some conversion to a one phase area on reheating to 1600 degrees, holding at 1600°C. for an hour, and then letting the sample furnace cool. Alloys of this composition are apparently one phase only up to 1800°C. They can be easily converted to UC and  $UC_2$  by heating to some temperature above 1800 degrees for a short period of time and then cooling in the furnace.

Since the positions of the X-ray diffraction powder maxima show little shift with overall composition of the sample the authors state that the  $U_2C_3$  structure covers "a very narrow single phase field".

Although there is a narrow single phase field below 1800 degrees Centigrade, the microstructures obtained at Ames by the author definitely show that there must be a fairly extensive single phase field (extending over approximately 9 atomic per cent) at some temperature between 1800 degrees and the melting point. See section IV F. for a further discussion of this region.

E. Melting Points of UC, U<sub>2</sub>C<sub>3</sub>, and UC<sub>2</sub>

The melting point values for the compounds in this system were

Table 2

Melting Points of Uranium Carbides

Compound	% C (Theoretical)	By analysis % C of sample used	Melting point
UC	4.80	2.7%	2250-2300°C
U <sub>2</sub> C <sub>3</sub>	7.03	6.95	2350-2400
UC <sub>2</sub>	9.16	9.18	2350-2400

approximated by heating samples in a vacuum to successively higher temperatures and examining them for signs of fusion. The samples were roughly tetrahedral in shape, approximately 8 mm. high and 4-5 mm. wide at the base, and were mounted on a graphite disk cut so that there was as little contact as possible between the sample and its support. This method is not a very accurate one because the carbon present may change

the composition of the sample and therefore its melting point. It was adopted because it was the simplest feasible method which suggested itself with the equipment available at the time of these determinations. The melting points determined in this manner are listed in Table 2.

F. Equilibrium Relationships among UC, UC<sub>2</sub> and UC<sub>3</sub> (23)

In order to examine this portion of the system a series of carbides

Table 3

Distribution of Regions in High Carbon Alloys

Figure	Composition Wt% Carbon	Number of regions visible	Regions
19	4.8	1	UC
20	5.2	2	UC & delta
21	6.59	1	delta
	7.04	1	delta
22	8.36	2	delta + epsilon
23	9.16	1	epsilon

varying in carbon content from 4.8-13.0 wt% was prepared. In each of these samples, except for the monocarbide (4.8 wt%), two phases were visible which X-ray analysis showed to be UC and UC<sub>2</sub>. The distribution of these phases varied, however, as the composition changed and definitely separate and distinct regions could be observed. (See Figures 18-22) A region may be defined as an area containing the same phases

in the same proportion throughout. Table 3 gives a summary of the number and kinds of regions found in each sample.

As the carbon content increases one notes the regular alternation of regions. Examination of the microstructures shows that there is little doubt that each region must be a one phase area at some high temperature. Assuming each region to be a one phase area one sees the regular 1, 2, 1, 2 alternation of the number of phases visible which is characteristic of any phase diagram. In Figure 18 the only phase present is the dark etching UC. In Figure 19 the phases present at high temperature would be the dark UC and the delta phase formed from the striated region visible in the photomicrograph. In Figure 20 the striated Widmanstatten structure region would appear as a one phase area (delta phase). In Figure 21 the broad lined region would be present as delta phase and fine lined structure would be the epsilon phase. In Figure 22 the laminated region would be a one phase area (epsilon phase).

As noted above in this report all attempts to locate the temperature at which the delta phase breaks down to UC and UC<sub>2</sub> were unsuccessful. Yet its Widmanstatten structure is characteristic of the breakdown of a one phase area into two phases. The failure of all quenching experiments to retain the delta phase indicates, therefore, that the change from a one to a two phase area in this system is an extremely rapid one. In the phase diagram presented in this report (Figure 28) 2000°C has been arbitrarily set as the temperature at which the delta

solid solution breaks down. Because of its extreme rapidity it is doubtful that the change occurs at a temperature lower than 2000°C. The exact location of the transformation line is not now known, however, with any certainty.

In order to determine whether or not a higher carbide than UC<sub>2</sub> existed, samples containing up to 13 per cent carbon were prepared by heating uranium-carbon mixtures up to 2800°C. (23) The microstructure of these samples (Figures 23 and 24) consisted of precipitated carbon in UC<sub>2</sub> plus a few areas of carbon which had never been in solution, showing that molten UC<sub>2</sub> dissolves carbon and that this carbon is precipitated on cooling and does not form a carbide higher than UC<sub>2</sub>. X-ray study showed no carbide other than UC<sub>2</sub> to be present and when the UC<sub>2</sub> was dissolved and the insoluble residue examined, it was found to be graphite, showing beyond a reasonable doubt that UC<sub>2</sub> is the highest stable carbide of uranium.

The solubility of carbon in liquid UC<sub>2</sub> at temperatures above 2400°C has been determined by Chiotti by holding samples of molten UC<sub>2</sub> at the desired temperatures in a graphite crucible and analyzing the resulting alloy for carbon much as the liquidus between uranium and UC was determined. (24) The data for this determination are shown in Figure 29. The 3000°C temperature was obtained by extrapolating beyond the calibrated range of an optical pyrometer and is a rough figure.

X-ray photographs have shown that the lamellar phase present in slowly cooled UC<sub>2</sub> samples is UC (see X-ray section). On quenching UC<sub>2</sub>

from 2400°C, this lamellar structure disappears and only one phase is present. (Figure 29) Accompanying this change in microstructure is a decrease in the lattice spacings of UC<sub>2</sub>. The UC X-ray diffraction pattern and the lamellar microstructure reappeared when these quenched samples were annealed at 1000°C and 2000°C. It seems fairly certain, therefore, that there is some solid solubility of UC in UC<sub>2</sub> above 2000°C.

#### V. Hardness of U-C Alloys from 0-4.8% Carbon

Rockwell hardness values for alloys up to 4.8 wt per cent carbon are given in Figure 30. Due to the rather large UC dendrites in the samples, hardness values varied considerably over the surface of some of the test pieces. The alloys beyond 4.8 per cent carbon could not be tested with a Rockwell tester because of their brittleness.

#### VI. X-ray Study of the Uranium-Carbon System

##### A. Uranium Monocarbide (UC) (25,26)

X-ray analysis of inclusions separated from uranium carbon alloys of less than 4.8 wt% showed that the X-ray diagram consisted essentially of maxima from a single, face-centered cubic phase,  $a_0 = \text{ca. } 4.9 \text{ \AA}$ . The separation of these inclusions is described in section I B. Chemical analysis of the separated dendrites closely approximated the value for uranium monocarbide and the X-ray data left no doubt that the chemical analyses were not fortuitous but that the dendrites are a definite chemical compound, uranium monocarbide.

The lattice spacings of the purest samples of uranium monocarbide (prepared from uranium and carbon in an atmosphere free of nitrogen and oxygen) were determined by using a symmetrical, self-focusing, back reflection camera of five centimeter radius and copper K radiation. The lattice parameters have been corrected by Cohen's extrapolation as recommended by Jette and Foote.

Spacings varying from  $4.951 \text{ \AA}$  to  $4.948 \text{ \AA}$  were obtained in various samples. Examination of spacings in samples containing excess carbon and in samples containing excess uranium showed that there was no consistent variation of spacing with carbon content but that there did seem to be a lowering in spacing in samples when nitrogen and oxygen contamination were appreciable. This point is discussed more fully below. It is believed that the most reliable value for the lattice parameter of the monocarbide is the highest that has been obtained, namely,

$$a = 4.951 \text{ \AA} \qquad \rho = 13.63 \text{ g/cc}$$

Uranium monocarbide contains four uranium atoms in face-centered positions. The probable structure is consequently either the sodium chloride or the zinc blend structure. A comparison of the intensity of reflections (420) and (331) showed that the more probable structure which corresponds to the intensity distribution is the sodium chloride structure.

#### B. Nitrogen and Oxygen Contamination of UC (27)

Recently uranium monoxide and mononitride have been discovered.

Both of these compounds are isomorphous with UC and all three have nearly equal lattice spacings. (Spacings are UN = 4.88 Å, UO = 4.91 Å, UC = 4.95 Å). Conditions are therefore ideal for mutual replacement of carbon, nitrogen and oxygen in a mono-uranium compound.

In all preparations where there was not a careful exclusion of nitrogen and oxygen the spacing of the monocarbide was lower than when prepared in an inert atmosphere. In order to confirm this point equimolar amounts of monocarbide and mononitride were heated together at 1950°C for fifteen minutes. Analysis of the resulting product showed that the spacings of each compound were changed toward a common average. The results were as follows:

	UC	UN
Initial Spacing	4.947 ± .001 Å	4.883 ± .001 Å
Final Spacing	4.921 ± .001 Å	4.917 ± .001 Å

The reflections in the heated sample were resolved in a self-focusing back reflection camera.

Probably continued heating would have caused a complete conversion to one phase. Similar experiments were not carried out with uranium monoxide due to the difficulty of preparing this compound but there is little doubt that replacement of carbon by oxygen is possible.

Reasoning from the evidence presented above it is likely that a major portion of oxygen and nitrogen impurity in a uranium casting is contained within the uranium carbide dendrites.



C. Uranium Sesquicarbide,  $U_2C_3$  (28)

All X-ray diagrams of samples corresponding to the stoichiometric composition of uranium sesquicarbide show that at room temperature it consists of a mixture of uranium mono- and di-carbide. Uranium sesquicarbide has been reported in the literature as a definite compound but no microscopic or X-ray evidence has ever been presented to date for the high temperature form.

There is, however, good evidence that at very high temperatures  $U_2C_3$  exists as a definite compound. When material of this composition (7.04 wt% C) is melted and allowed to freeze, what appear to be single perfectly cubic crystals are formed. A "single crystal" X-ray diagram obtained from one of these crystals showed that it consisted of uranium mono- and di-carbide phases which had crystallized with their axes parallel. From the form of the macro-crystals uranium sesquicarbide is assumed to be cubic but since it is stable only at very high temperatures (see section IV D) there is little hope at present of obtaining an X-ray diagram from this compound unless a high temperature X-ray diffraction apparatus is used.

Mallett, Gerds and Vaughan report the following crystallographic data for the single phase sesquicarbide obtained by them below 1800 degrees Centigrade. The unit cell is body centered cubic with  $a_0$  equal to 8.008 Å. Calculated density is 12.88 g/cc. The space group is  $I4_3d$ . Only the uranium positions were determined and they are in position 16 (c) of the space group as listed in the Internationale Tabellen zur Bestimmung von

Krystallstrukturen (31) with the X parameter equal to 0.20.

D. Uranium Dicarbide, UC<sub>2</sub> (29)

As reported in 1931 and confirmed in this laboratory uranium dicarbide is body centered tetragonal and its structure is isomorphous with that of lanthanum carbide.

Both X-ray analysis and microscopic study showed that when uranium dicarbide is slowly cooled from high temperature or when quenched samples are annealed, the dicarbide contains monocarbide in appreciable quantities. Even when a considerable excess of free carbon is present the monocarbide phase is noted. On the other hand if the dicarbide is quenched from temperatures above 2400°C no monocarbide phase is present.

X-ray spacings of UC<sub>2</sub> depend also on thermal treatments. Table 4 contains spacings of dicarbide treated in various ways. Worthy of note is the fact that the carbide spacing is lower on samples quenched from very high temperature.

All of the samples in Table 4 contain excess carbon (i.e. carbon in excess of the stoichiometric composition for UC<sub>2</sub> 9.16 wt%). Enough of this excess carbon was present to be easily visible under the microscope. Hence, all spacings are for dicarbide saturated with carbon. The melting point of the dicarbide is approximately 2375 ± 25°C.

A review of chemical analyses, X-ray spacings, and microscopic examination leads to the conclusion that at some temperature below 2400°C uranium dicarbide is unstable and decomposes into monocarbide and carbon. It also appears that the spacing of the dicarbide is decreased

by carbon solubility and that the carbon solubility is appreciable in the liquid state using with increasing temperature but is much less in the solid state falling off to an inappreciable quantity by 1000°C.

The decrease in uranium dicarbide lattice parameter with increasing carbon content shows that the dicarbide is probably not an interstitial solution of carbon in uranium. If it were an interstitial solution of carbon in uranium one would expect an increase in lattice parameter with increasing carbon content.

Table 4  
Lattice Parameters of Quenched Samples of UC<sub>2</sub>

Treatment of UC <sub>2</sub>	Lattice Parameters	
	(a)	(c)
Cooled slowly to room temp.	3.517 Å	5.987 Å
Quenched from 1000°C	3.517	5.985
Quenched from 2400°C	3.509	5.962
Quenched from 2700°C	3.505	5.951

It seems best to regard the dicarbide as consisting of relatively negative C<sub>2</sub> ions with small positive uranium ions contained within the interstices of the negative ions. A decrease in lattice spacing with increased carbon content could then be ascribed to a deficiency of uranium in the carbide leaving some of the interstices vacant with a consequent shrinkage in the molecule. A similar phenomenon occurs in

uranium dioxide whose lattice spacing decreases as the oxygen content is increased.

If the above interpretation is correct the larger values of the dicarbide spacing correspond to pure dicarbide. Hence, for

$$\text{UC}_2 \quad a = 3.517 \text{ \AA} \quad c = 5.987 \text{ \AA} \quad \rho = 11.68 \text{ g/cm}^3.$$

The substance of this X-ray section is taken from a report by the Ames X-ray group consisting of Dr. R. E. Rundle, A. S. Wilson and N. C. Baenziger. A more complete discussion of the X-ray structures of uranium carbides is given in "X-ray Analysis of the Uranium-Carbon System" in Volume XI B of M.P.R. and also in reference (42).

## VII. Polishing and Etching

To study microstructures samples were ground through a 4/0 Behr-Manning emery paper and then polished on a Gamal or billiard cloth with a soap suspension of levigated alumina.

For low carbon (0-4.8 wt% C) samples an electrolytic polish (14) was used consisting of

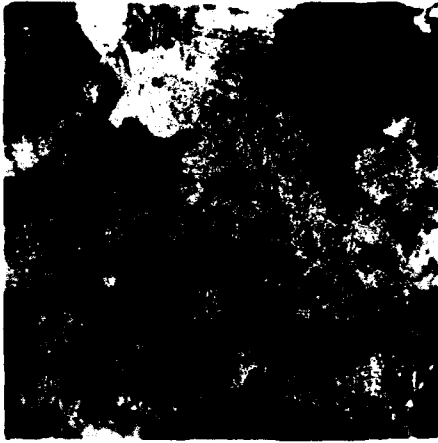
5 parts 85% phosphoric acid

5 parts ethylene glycol

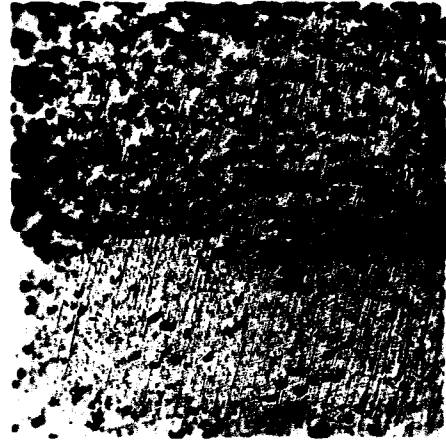
8 parts ethyl alcohol

The current density usually used was 3-5 amp/sq.dm. for about 10 minutes. Good results were obtained using 18 volts and a bath temperature of 30-50°C. Using a lower current density, this bath served as an etch. Oxalic acid (10% solution) and 2% nitric acid were also used as electrolytic etches for samples in the 0-4.8 wt% region.

The carbides could be satisfactorily etched by a short dip in 1-1  $\text{HNO}_3$  solution which gave high contrast. Finer detail was brought out by a 10% oxalic acid electrolytic etch.



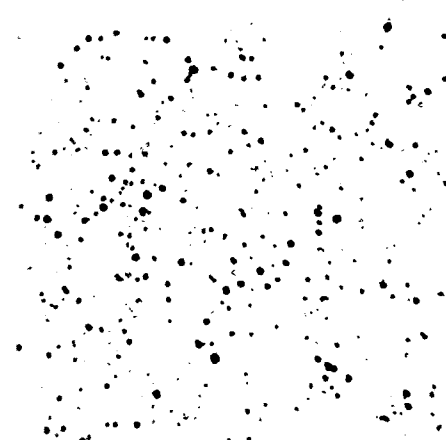
1



2



3



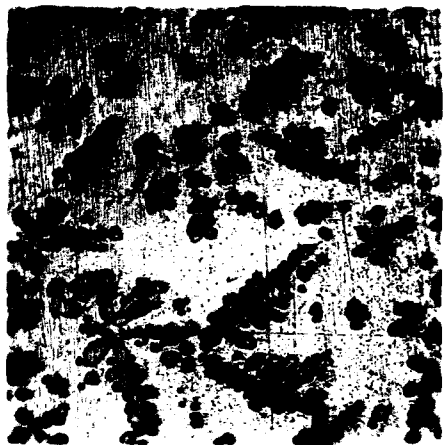
4

Fig. 1 - Uranium metal of high purity. 10% oxalic acid electrolytic etch. X 10.

Fig. 2 - Segregation at top of production ingot. Top 0.325 wt% C. Bottom 0.123 wt% C. Unetched. X 50.

Fig. 3 - 0.0065 wt% C. Uranium plus UC inclusions. Fine material in background is due to Fe impurity. Electrolytic polish. X 50.

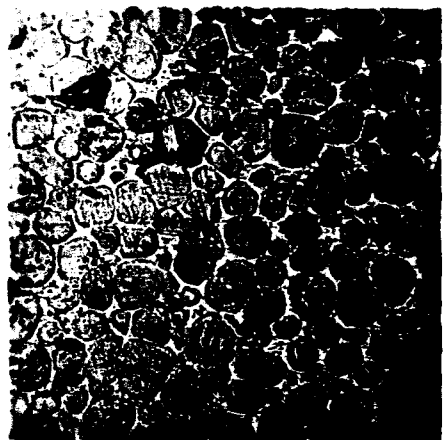
Fig. 4 - 0.0443 wt% C. Uranium plus UC inclusions. Electrolytic polish. X 50.



5



6



7



8

Fig. 5 - 0.203 wt% C. Uranium plus UC inclusions. Unetched. X 50.

Fig. 6 - 0.70 wt% C. Uranium plus UC inclusions. Unetched. X 10.

Fig. 7 - 2.33 wt% C. Uranium in grain boundaries. UC inclusions.  
Electrolytic polish. X 200.

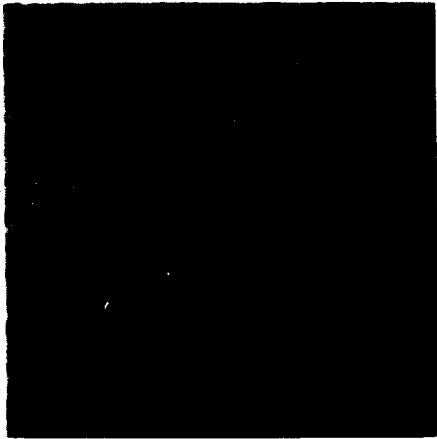
Fig. 8 - 3.12 wt% C. Uranium in grain boundaries. UC inclusions.  
Electrolytic polish. X 500.



9



10



11



12

Fig. 9 - 4.83 wt% C. UC. Dark spots are voids. 10% oxalic acid electrolytic etch. X 500.

Fig. 10 - 4.8 wt% C. UC inclusions separated from alloy containing 1.50 wt% C. X 10.

Fig. 11 - 0.41 wt% C. Upper zone of U-UC briquette heated to 1700° C. Electrolytic polish. X 100.

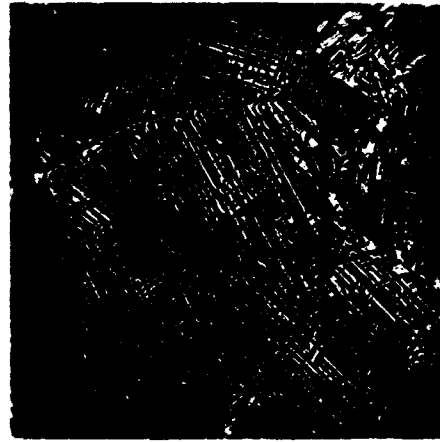
Fig. 12 - 0.41 wt% C. Lower zone of U-UC briquette heated to 1700° C. Electrolytic polish. X 100.



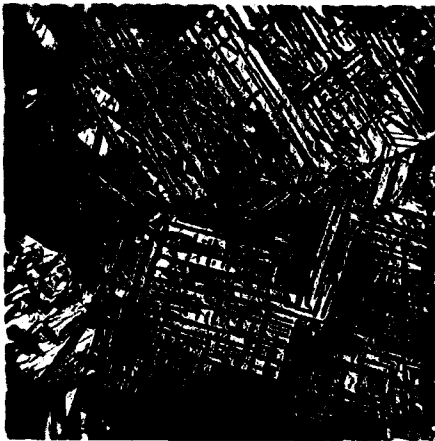
$U_2C_3$



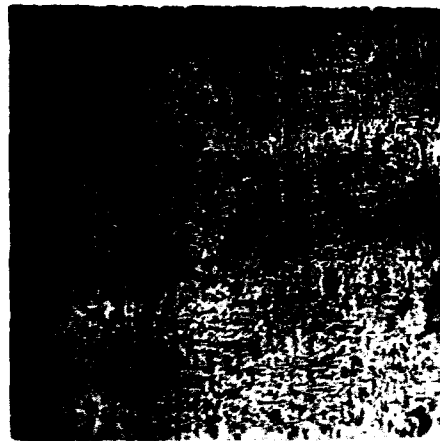
13



14



15  $U_2C_3$



16

Fig. 13 - 0.41 wt% C. U-UC briquette heated to 1950° C. Electrolytic polish. X 100.

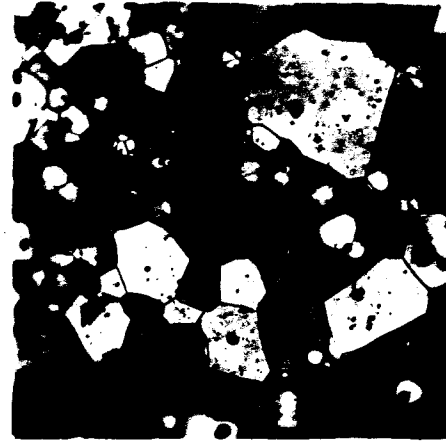
Fig. 14 - 7 wt% C (approx.). Typical decomposed delta phase Widmanstatten structure. 10% oxalic acid electrolytic etch. X 50.

Fig. 15 - Same sample as shown in Fig. 14. 10% oxalic acid electrolytic etch. X 100.

Fig. 16 - 7.03 wt% C. Delta phase quenched from 1900° C. 10% oxalic acid electrolytic etch. X 200.



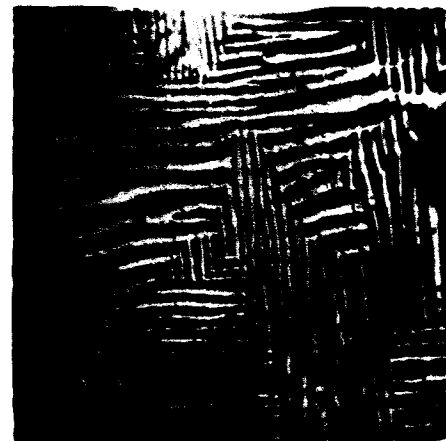
17



18



19



20

Fig. 17 - Same sample as shown in Fig. 16. 10% oxalic acid electrolytic etch. X 500.

Fig. 18 - 4.83 wt% C. UC. Dark spots are voids. 10% oxalic acid electrolytic etch. X 500.

Fig. 19 - 5.2 wt% C. UC and decomposed delta phase. Dark phase is UC. Banded areas are decomposed delta phase. 1-1 HNO<sub>3</sub> etch. X 500.

Fig. 20 - 6.59 wt% C. Decomposed delta phase. Bands are UC and UC<sub>2</sub>.  
1-1 HNO<sub>3</sub> etch. X 500.



21



22



23



24

Fig. 21 - 8.36 wt% C. Decomposed delta and epsilon phases. Broad lined areas are decomposed delta. Fine lined material is decomposed epsilon. 1-1 HNO<sub>3</sub> etch. X 500.

Fig. 22 - 9 wt% C (approx.). Decomposed epsilon phase. 1-1 HNO<sub>3</sub> etch. X 500.

Fig. 23 - 11.0 wt% C. Decomposed epsilon phase and C. White areas are graphite inclusions. 10% oxalic acid electrolytic etch. X 500.

Fig. 24 - Decomposed epsilon phase and C. Dark inclusions are free graphite. Unetched. X 250.



Fig. 25 - 10.66 wt% C. Epsilon phase and C. Sample quenched from 2700° C. No laminations due to decomposed epsilon phase are visible in this sample even at 1000 X. 1-1 HNO<sub>3</sub> etch. X 500.



Fig. 26 - Quenched sample, shown in Fig. 25, annealed at 2200-2300° C. for 20 minutes. 10% oxalic acid electrolytic etch. X 250.

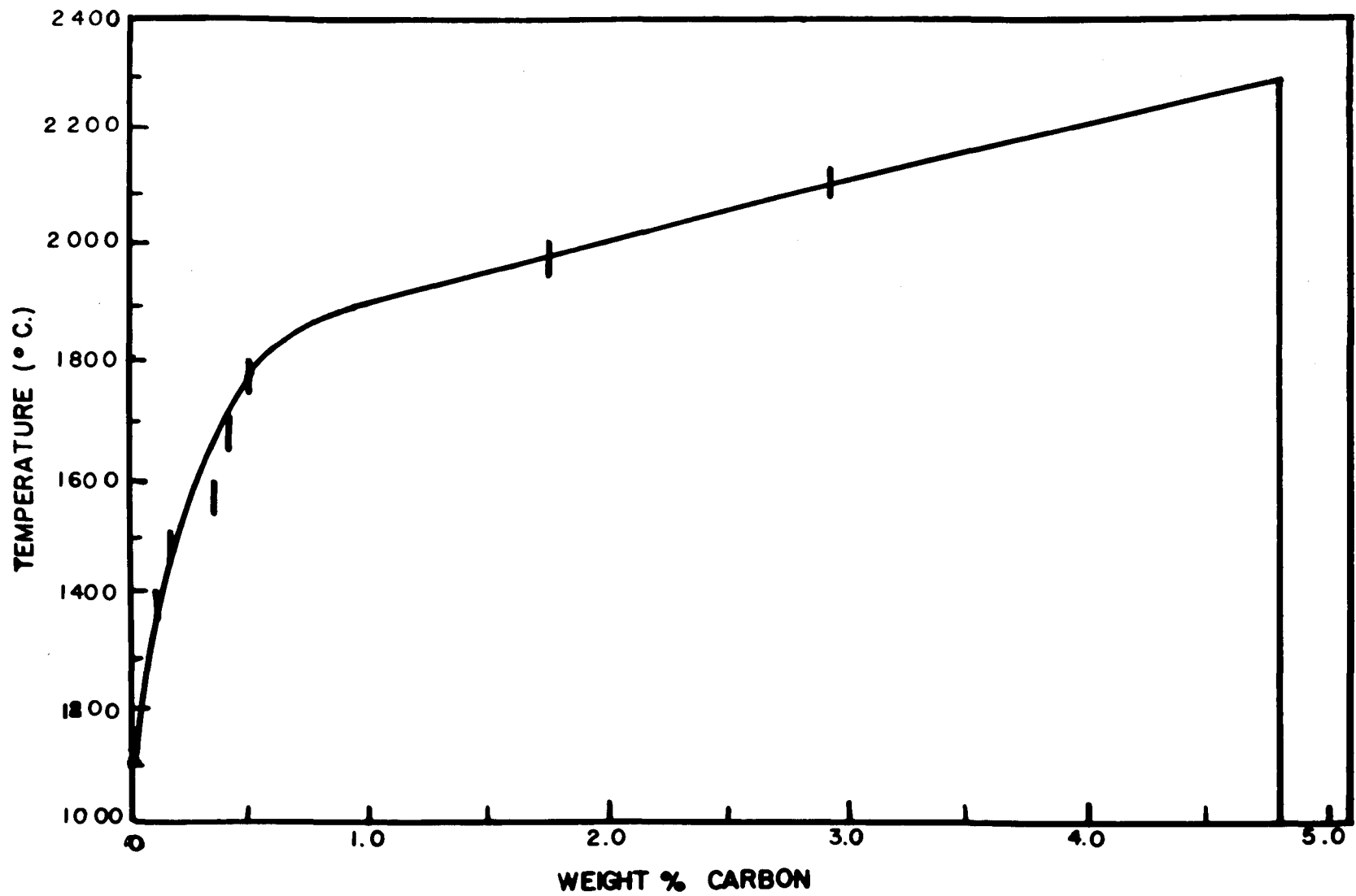


Fig. 27 - Liquidus line of uranium-carbon system from 0-4.8 wt% carbon.

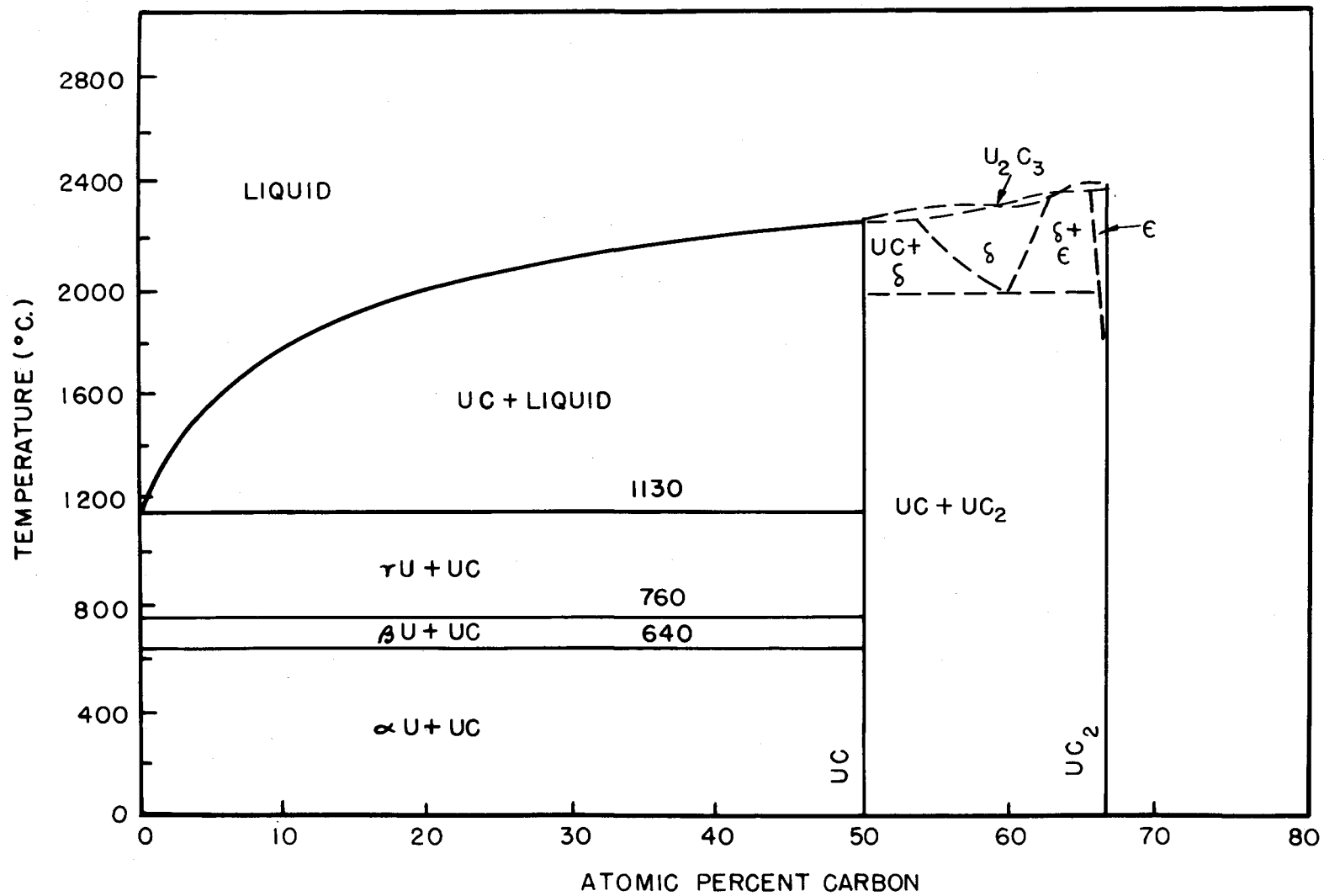


Fig. 28 - Phase diagram of the uranium-carbon system.

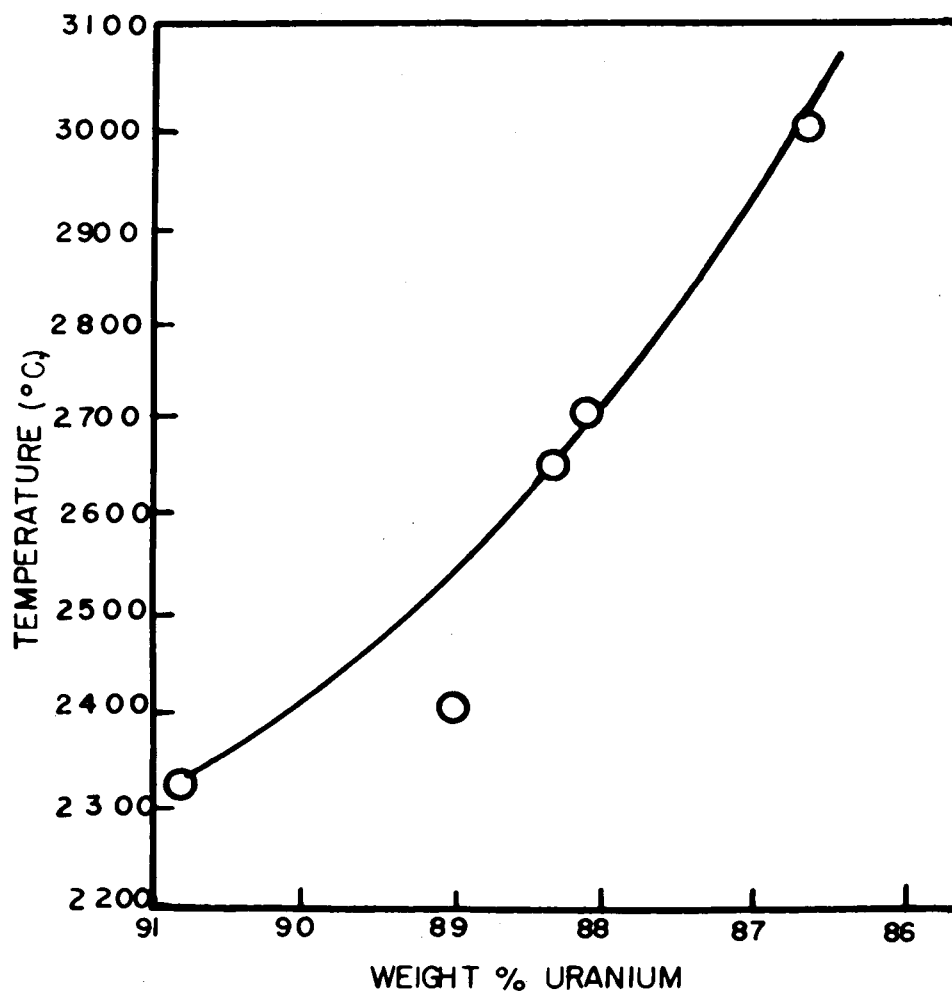


Fig. 29 - Solubility of carbon in liquid  $UC_2$ .

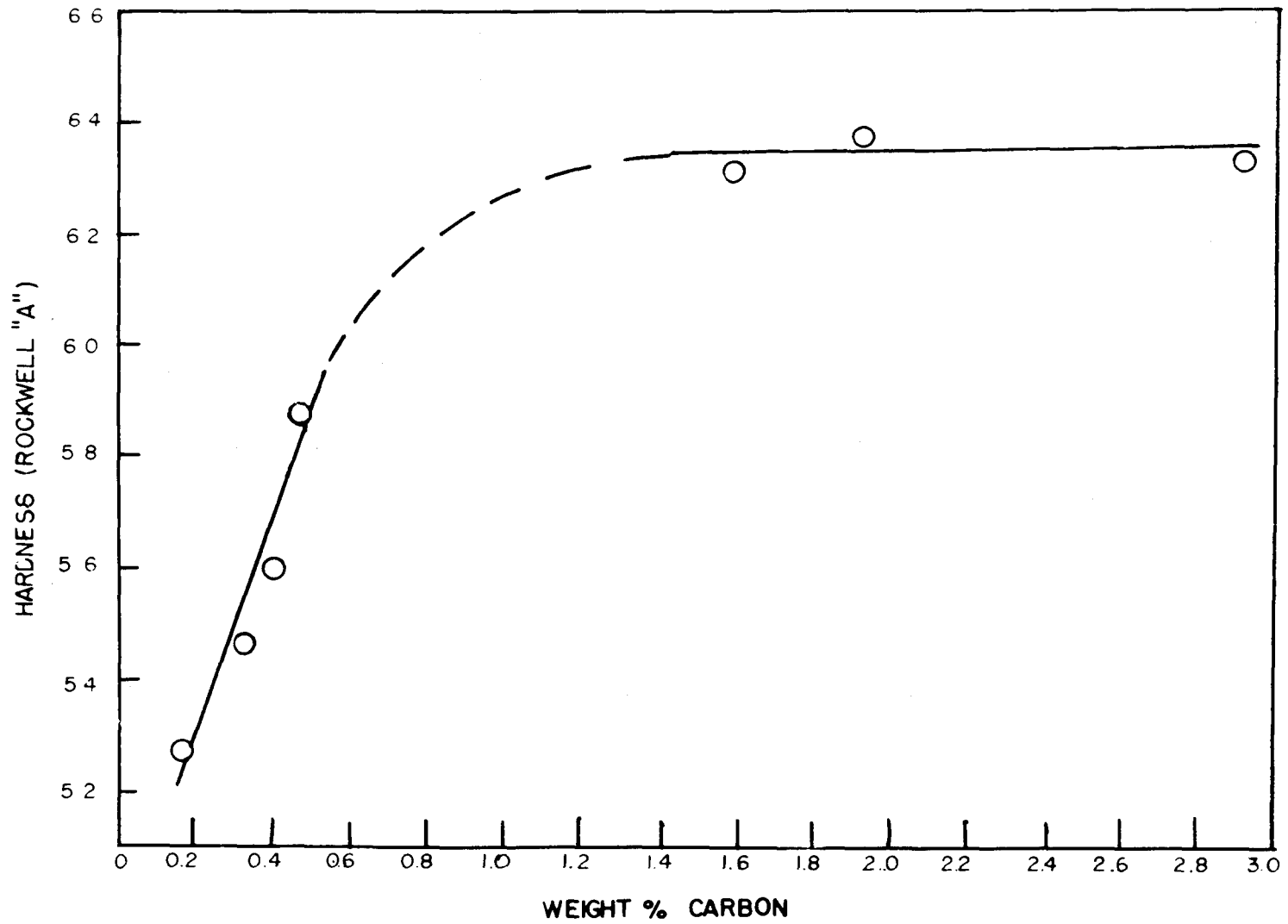


Fig. 30 - Rockwell "A" hardness of uranium-carbon alloys from 0-4.8 wt% carbon.

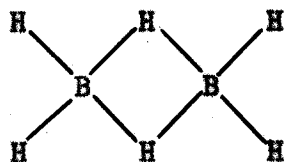


## THE STRUCTURE OF DIMETHYLBERYLLIUM AND ITS BEARING ON CHEMICAL VALENCE

### I. Introduction and Historical Background

In recent years there has been much interest in electron-deficient compounds. Electron-deficient compounds are those which do not contain enough electrons in the valence shells of the constituent atoms to provide an electron pair for every bond which may be assigned, in the conventional manner, to adjacent pairs of atoms. The compound of this type which has been investigated most thoroughly, by a wide variety of experimental methods, and which has been discussed at greatest length from the theoretical viewpoint is diborane ( $B_2H_6$ ). Since discussions of the diborane molecular structure serve as a prototype for many discussions of electron-deficient compounds we shall examine this compound in some detail.

Practically every remotely reasonable type of structure attainable by permutations in the positions of two boron atoms and six hydrogen atoms has been proposed for diborane (32), but experimental evidence has supported only two of these, namely, the ethane and the bridge structures. The ethane structure is similar to the arrangements of the carbons and hydrogens in ethane, but with the boron atom replacing the carbon atom. The bridge structure, first proposed by Dilthey (33) and Core (34), is shown below. Its configuration is similar to that proposed for the aluminum chloride dimer.



The experimental evidence for each of these structures is given below.

Chemical Evidence - Diborane reacts with electron donors to form molecules with no electron deficiency, but this sort of reaction does not give any information in regard to the original configuration. The fact that at the most only four of the six hydrogen atoms can be substituted by methyl groups indicates that perhaps the two unsubstituted hydrogen atoms occupy a unique position in the molecule. This supposition is more in harmony with the bridge than with the ethane-like configuration.

Crystal Structure - The X-ray diffraction determination of the crystal structure of the solid by Mark and Pohland (35) has often been quoted as support for the ethane structure, but examination of their paper shows that although the boron positions were approximated from the intensity data, the hydrogen positions were merely assumed.

Electron Diffraction - Electron diffraction data obtained by Bauer (36) was originally interpreted by him as favoring strongly the ethane structure. Subsequently, Bauer and others (36) showed that the data could also be satisfactorily interpreted on the basis of a bridge structure.

Shand (37) investigated tetramethyldiborane by electron diffraction and found that the data were better explained by an ethylene-like structure than an ethane-like structure. This evidence supports the bridge model.

Infra Red and Raman Spectra - The Raman spectrum of liquid diborane was investigated by Anderson and Burg (38). The infra red spectrum of the gas was investigated by Stitt (58) and Price (40). Early attempts were made by Stitt to interpret his data on the basis of the ethane model by the use of various ad hoc assumptions about low-lying energy levels and resonance splitting. Even with this method of approach frequency assignments were not very satisfactory.

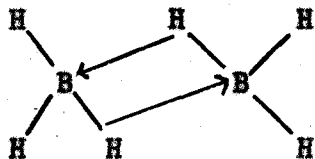
Bell and Longuet-Higgins (39), Price (40), and Webb, Neu and Pitzer (51) have shown that the vibrational data are consistent with a bridge model but not an ethane model.

Specific Heat Data - Stitt (58,59) used his specific heat data to calculate the barrier to rotation of the hydrogens in diborane. These calculations led to a potential barrier of 4000-6000 cal./mol. for diborane in contrast to a barrier of only 3000 cal./mol. for ethane. Taking supposedly low-lying energy levels (needed to explain the infra red data on the ethane model) into account he obtained an even higher barrier to rotation of the hydrogens in diborane. Longuet-Higgins and Bell (39) point out that potential barriers of this type are due to interactions of hydrogens and/or partial bond character in the central link. On either basis one would expect less hindered rotation in di-

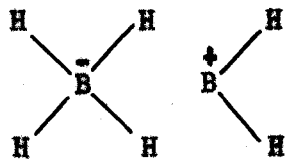
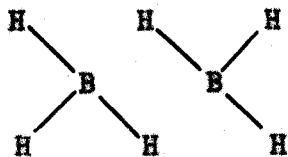
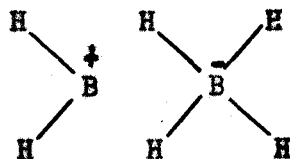
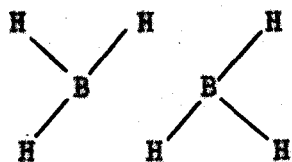
borane than in ethane since the hydrogens would be farther apart than in ethane and the amount of double bond character in a boron-boron bond should be less than in carbon-carbon bond.

In addition to Longuet-Higgins and Bell (39), Nekrassov (41), Sirkin and Diatkina (42), and Pitzer (43) reviewed the experimental data and concluded that the bridge structure is the most probable one. Pitzer described the bridge bonds as "protonated double bonds". His ideas were similar to those of Wiberg's (32), suggested years before, except that Pitzer was more specific about the location of the bridge protons. Pitzer's description implied that the  $sp^2$  orbitals of each boron atom were involved in two B-H bonds and one B-B bond. The two lobes of the remaining p orbital on each boron atom overlap with the s orbitals of hydrogen above and below the plane of the molecule. Rundle (44) has pointed out that this orbital arrangement leaves one electron pair to bond both bridge hydrogen atoms, so that they have a formal charge of  $+\frac{1}{2}$  and might be expected to be weakly bound and acidic. Rundle suggested the use of tetrahedral orbitals of boron to form B-H bonds with the s orbital of hydrogen. If Rundle's arrangement of orbitals is correct no formal charges are necessary for the hydrogen atoms, and the hydrogen atoms are bound more firmly than according to Pitzer's suggestion. The type of bonding suggested by Rundle also helps to explain Burg's observation (60) that no acidic hydrogens are present in diborane.

Walsh (45) favored a type of bonding which may be represented as follows



One of the consequences of Walsh's proposal is that the terminal hydrogens are not coplanar which is in conflict with the experimental evidence obtained from infra red and Raman spectra. Among other suggestions was that of Burawoy (46) who proposed that the association in diborane is caused by hydrogen bonding. The electronegativities of hydrogen and boron are so nearly alike, however, that one would not expect a very strong hydrogen bond to form in diborane. Several authors (47,48, 49) have suggested a resonance formulation of the bridge bond. The hypothetical separate resonating structures are shown below.

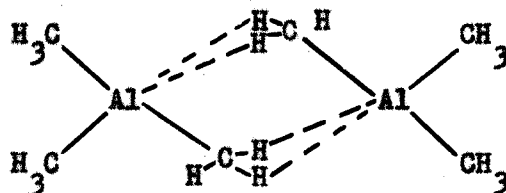


Although it is usually not considered that the two parts of a molecule can be held together solely by resonance stabilization, theoretically there is nothing to prevent this from happening.

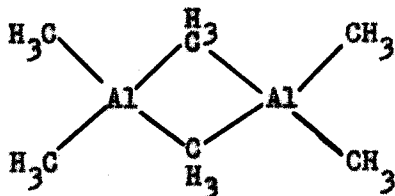
Mulliken (52) has applied the molecular orbital method to the structure of diborane. His early treatment, based on the ethane model, predicted that this compound should be paramagnetic. This prediction was not borne out experimentally. Utilizing Pitzer's suggestion (43) that the structure for diborane could be derived from ethylene by imagining the removal of a proton from each carbon nucleus, Mulliken has enumerated the molecular orbitals and found that they are similar to those of ethylene except that the  $\pi$  orbitals now include the protons as well as the boron nuclei. Mulliken also found that there should be considerable overlap of the  $2p$  orbitals of boron even at single bond distances, which makes the existence of a double bond seem very probable.

Lately it has been shown (57) that electron-deficient bonding is not a rare occurrence. Such bonding is to be expected whenever certain rules, which will be presented later, are satisfied (56).

Trimethyl aluminum is known to exist in the dimeric form and, therefore, the aluminum alkyl dimer must contain electron-deficient bonds. A bridge structure has been proposed for this molecule also, but opinions differ in reference to the type of bonding present in the bridge. Pitzer and Gutowsky (53) proposed the following structure for this compound.



Pitzer and Gutowsky suggested that the negative carbon atom is attracted to the positive aluminum core. Rundle has suggested that the hydrogen atom between aluminum and carbon must interfere with this attraction and in fact the weak C-H dipole has its positive end directed toward the aluminum. The bond cannot be a "protonated double bond" since it is unlikely that aluminum would violate the octet rule. Although the polar nature of the bridge bond proposed by Pitzer and Gutowsky is not unlike a hydrogen bond, Rundle states that it cannot be as strong as such a bond between very electronegative elements, and, in fact, he doubts that such a bond would be strong enough to overcome the decrease in entropy accompanying dimerization. As an alternative to Pitzer and Gutowsky's ideas Rundle (56) has proposed the following structure for the aluminum alkyl dimer. This structure will be discussed in the light of results obtained for dimethyl-beryllium in a later section of this thesis.



Another interesting electron-deficient compound is tetramethylplatinum whose structure was determined by Rundle and Sturdivant (54). Since this compound is a solid at room temperature the authors were able to determine its structure by means of X-ray diffraction which is less ambiguous than are other methods for the determination of molecular structure. The tetramethylplatinum molecule is a tetramer with platinum atoms and methyl groups at the corners of a distorted cube. Bonded to each platinum are three external methyl groups. The bonding around platinum is essentially octahedral and presumably the bonding around the cube-corner carbons is octahedral also, although the hydrogen atoms cannot be located by X-ray methods in this particular compound. The platinum-platinum distance, 3.44 A., is much too long for any metal-metal bonding, so that metal-non-metal electron-deficient bonding is the only bonding holding the tetramer together. The question of the importance and necessity for metal-metal bonds in electron deficient compounds will be discussed more fully later.

Metals are regarded as examples of electron deficient bonding according to several points of view (61,62), but these ideas will not be discussed here. Rundle (55) has also shown that the formation and properties of various interstitial compounds can be understood on the basis of his theory of electron deficient bonding.

Rundle (56) has formulated some general rules which predict when electron-deficient bonding is to be expected. He explained electron-deficient bonding as caused by the great tendency of an element to use all of its low-lying orbitals in bond formation even at the expense of



a lower than normal electron density in some bonds. For such bonding to occur, the sum of the strengths of the electron-deficient bonds formed must be greater than the bond strengths of the alternative non-polymerised non electron-deficient compounds. On the basis of semi-quantitative calculations Rundle (57) has shown that for diborane the sum of the strengths of two electron-deficient B-H-B bonds is approximately 30% greater than for a single B-H bond.

According to Rundle (56) electron deficient bonding is to be expected in a compound, one of whose constituents has an excess of low energy orbitals over valence electrons and is, therefore, usually a metal and the other component is one which does not have a surplus of low energy orbitals over electrons and is, therefore, usually a non-metal. The electronegativities of these elements must not be too far apart since the stabilization of the electron deficient compound is a resonance stabilization and the gain in stability will be greatest if the electronegativities are equal. When the conditions described are fulfilled the non-metallic constituent will use one orbital to form more than one bond and so is, in a sense, orbital deficient. Since in many of the examples considered one electron pair occupies two bonds these bonds have been designated as "half bonds".

On the basis of the ideas presented above it would seem likely that in dimethylberyllium, a solid subliming at 200°C., the beryllium atoms would tend to form four tetrahedrally directed bonds to the carbon atoms and that the Be-C bonds would be electron deficient. There is some danger in such a prediction since trimethyl boron, which also

might be expected to polymerize, exists only as a monomer. Two reasons for the non-polymerization of trimethylboron have been advanced (56). One is that since boron has a small tetrahedral covalent radius the four membered ring formed would be under considerable strain. Beryllium has a larger covalent radius and, consequently, there would be less strain in a four membered beryllium-methyl ring. Another reason for trimethyl boron remaining monomeric is stabilization caused by the great hyperconjugation of the three methyl groups with the boron atom. Evidence for this hyperconjugation is given by Mulliken (52). In dimethyl beryllium there would be much less stabilization by hyperconjugation of only two methyl groups. Another factor, which may have some importance, is that in monomeric trimethyl boron only one stable low-lying orbital remains unused whereas in a hypothetical monomeric dimethylberyllium two stable orbitals would remain unused.

Considerations such as those outlined above led us to undertake determination of the structure of dimethylberyllium.

## II. Preparation of the Compound

Dimethylberyllium was prepared according to the method of Gilman and Schulze (63). In this method the compound is prepared by means of a double decomposition reaction between beryllium chloride and methyl magnesium iodide.

The apparatus used for the preparation is shown in Figure 31. This apparatus is basically the same as that used by Gilman and Schulze with the exception that here ground glass standard taper joints were

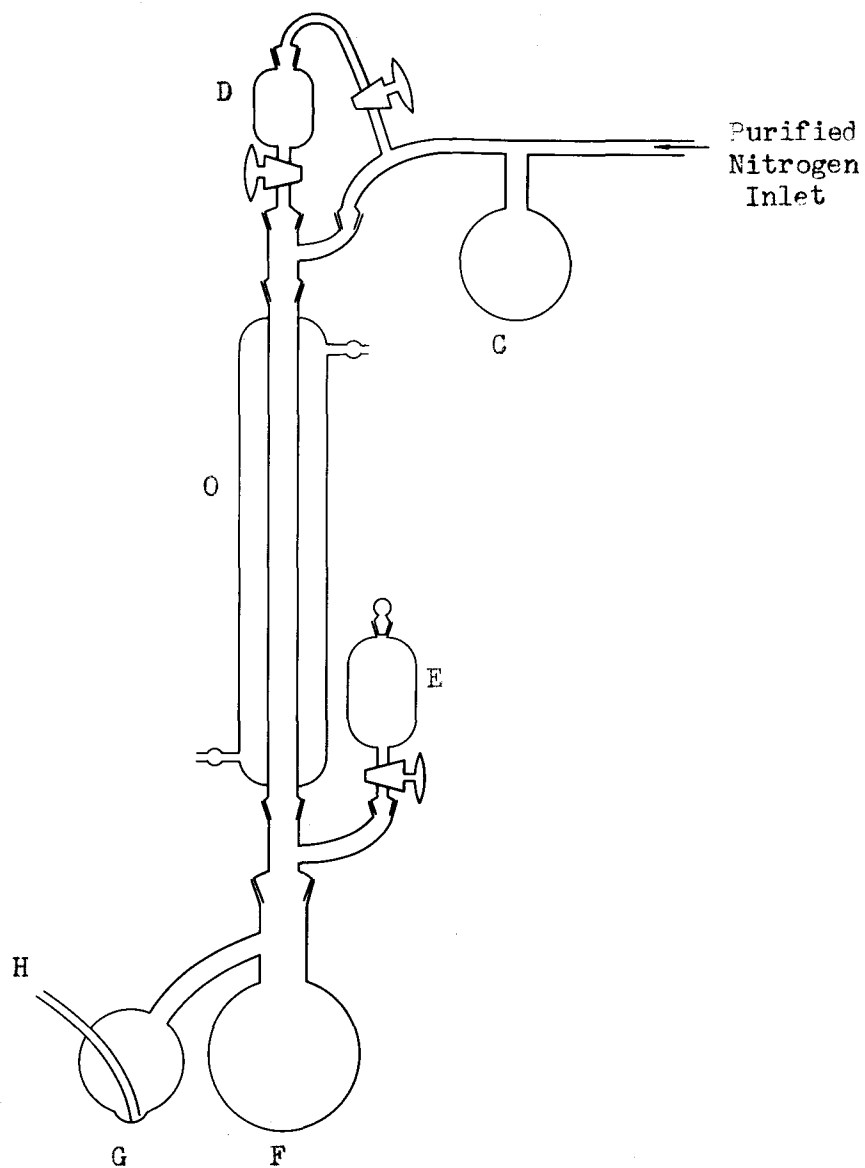


Fig. 31 - Apparatus for preparation of dimethylberyllium.

used throughout and there were some modifications in the manner in which solutions were added to the reaction flask F and also in the design of the receiving flask G. Due to the reactivity of the product with air and moisture all preparative operations were carried out under a nitrogen atmosphere. The nitrogen was purified by passing the dried gas over heated copper oxide and uranium nitride according to the procedure of Newton et al. (64).

Magnesium turnings were placed in reaction flask, F, and the apparatus was then assembled. After removal of air by passing nitrogen through the system and allowing the gas to exit at H, the apparatus was then sealed at H by attaching a piece of small bore rubber tubing closed by a screw clamp. Ethyl ether was added from the dropping funnel, E, and methyl iodide was then added from the same dropping funnel. After preparation of the methyl magnesium iodide, an ether solution of beryllium chloride was added from the dropping funnel, D. Excess ether was removed by stopping the circulation of water in the condenser, O, and heating the flask up to 150°C. This ether was collected in the cooled flask, C. After distillation of the ether the water was gradually allowed to cool the condenser, O, and the concentrated solution was distilled into the receiving flask, G. The solution in G could be concentrated by back distilling the excess of ether into F. In this method it is difficult, as pointed out by Gilman and Schulze, to know when the distillation is finished, but since only enough material for an X-ray examination was wanted yield was not a primary consideration, so that distillations were arbitrarily discontinued after about eight hours.

When the distillation was considered complete the tube, I, of the apparatus shown in Figure 32 was attached at H to the preparative apparatus. The newly attached section was evacuated by attaching it to a vacuum pump at M. The screw clamp at H was then opened and solution in G was quickly transferred into J. The tube, I, was then sealed off and the apparatus was attached to a vacuum system at M. Before attachment to the vacuum system the solution in J was cooled by a dry ice trichloroethylene bath. After attachment its temperature was allowed to rise gradually and the bulk of the ether distilled into a cooled receiver in another part of the system. After most of the ether had distilled white crystals were left behind which were purified of the last traces of ether by subliming them back and forth under a vacuum of better than half a micron. The crystals were then distilled into the capillaries at K, short lengths of which were then sealed off. The excess crystals were sealed off in the tubes above the capillaries for storage.

Obtaining material from storage tubes was somewhat of a problem. A drybox transfer under a nitrogen atmosphere was possible but whenever this procedure was followed there was always some loss of material due to oxidation. A better alternative adopted is shown in Figure 33. The tube containing the dimethylberyllium powder was placed at O between the two halves of a ball-and-socket standard taper joint. After evacuation of the apparatus the tube was broken by bending the ball-and-socket joint. The apparatus was then disconnected from the vacuum system and the glass and powder were poured into the reservoir, S.

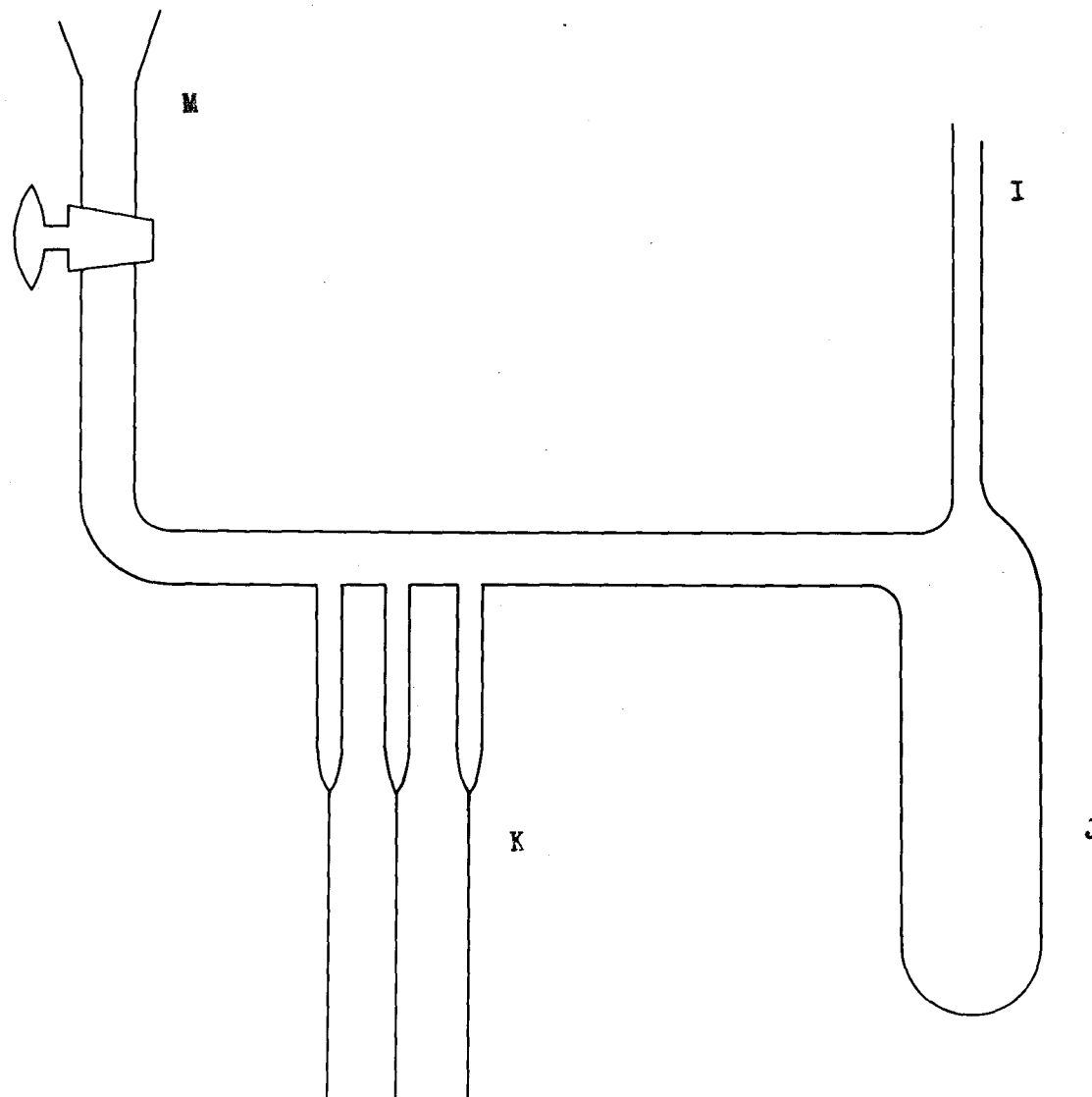


Fig. 32 - Apparatus for filling capillaries with purified dimethylberyllium.

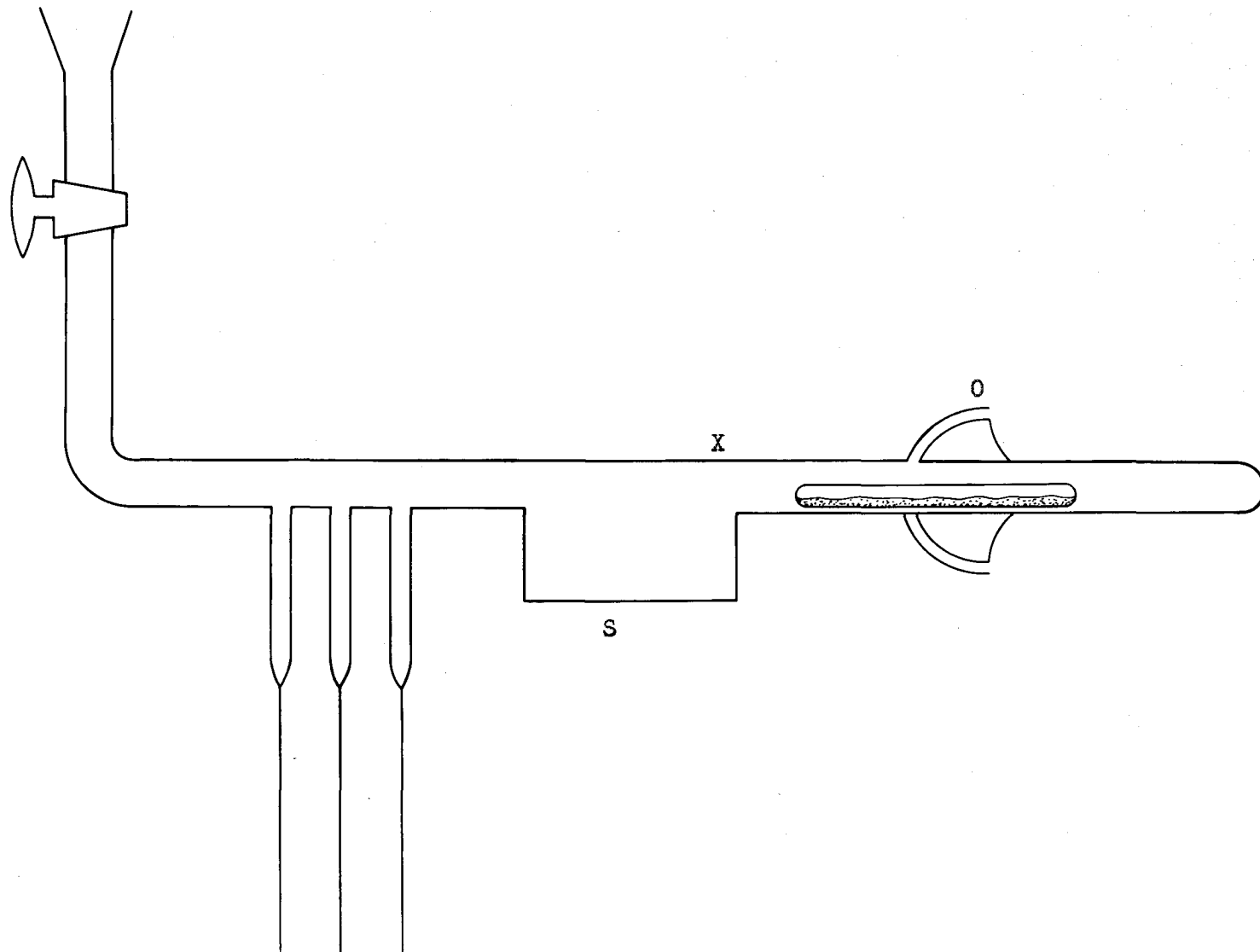


Fig. 33 - Apparatus for obtaining material from storage tubes.

The apparatus was then reconnected to the vacuum system, a seal-off made at X, and then the dimethylberyllium could be sublimed wherever wanted.

For obtaining X-ray powder diagrams, the capillaries, loaded as described, could be used directly, but since, as shall be shown, the crystal structure is too complex to be solved by powder methods alone, single crystals were necessary. The obtaining of single crystals of large enough size and located in the desired orientations in a capillary was the most time-consuming part of this investigation. The method first used was to grow the crystals in a thick tube by subliming them under a temperature gradient. The tube was then broken under a nitrogen atmosphere and the largest most perfectly formed crystals were worked into thin capillaries made of Pyrex or Lindemann glass. The capillaries were temporarily sealed by a bit of modeling clay and then were permanently sealed by a coating of pyseal wax over the modeling clay upon removal from the dry box. The crystal would usually stick to the clay and would be held firmly in place. Although some early Weissenberg diagrams were obtained from crystals mounted in this way this method was, in general unsatisfactory. One of the drawbacks was that there was always some slight oxidation of the crystal, although this was not too serious a factor. A more serious difficulty was in loading the extremely fragile capillaries in the dry box. The capillaries had to be made as thin as possible because all of the components of dimethylberyllium have a poorer X-ray scattering power than the oxygen, silicon and sodium of the glass. In handling, the thin capillaries were easily broken. The glass scattering could be lessened by using Lindemann



glass, a lithium beryllium borate glass, which was satisfactory enough for dry box transfers but was not satisfactory for attachment to the vacuum system. Another difficulty was the fact that this compound under sublimation grows in the form of needles which have a great tendency to form twinned crystals or aggregates of crystals which grow with their needle axes parallel with the other two major axes rotated with respect to each other. In practice, what appeared in the comparatively poor visibility of the dry box to be a single, large cross-sectioned needle often appeared under X-ray examination to be composed of many crystals. This situation was so bad with some crystals that it was possible to obtain what appeared to be a complete rotation X-ray diagram without rotating them at all.

Because of these difficulties the crystals were grown directly by sublimation in the capillaries in which they were to be mounted on the camera. The capillaries which contained a small amount of dimethylberyllium powder were put into a pyrex tube around which was wound nichrome wire with a decreasing density of turns per unit length of tube so that there was a fairly continuous temperature gradient along the length of the tube. The input voltage was controlled with a Variac and the progress in the growth of the crystal could be followed by placing the tube on the stage of a low powered microscope. Here the problem was isolation of a single crystal from all of the other crystals and crystallites present. By distilling slowly one could, if fortunate, start growing only a few crystals or, if very fortunate, one

crystal and by cautious heating around the crystal one could drive most of the other material away. Usually a little powder remained which added to the background on the X-ray film, especially at low angles. These crystals were fibrous in character and showed a tendency in many cases of growing as many thin crystals from a single nucleus rather than one single crystal. The growth properties of the crystals are consistent with the determined structure but they are of a nature which creates many experimental difficulties.

Two crystalline forms of this compound were noted under the polarizing microscope. The needle-like form, which is stable at room temperature shows only parallel extinction between crossed Nicol prisms. The other form shows extinction at all orientations between crossed Nicols and is therefore isotropic. This second form was obtained in some sublimations at first but after standing at room temperature would transform in approximately one-half hour into the birefringent form. On some samples of the isotropic form apparently square and triangular faces, perhaps corresponding to the (100) and (111) faces of a cube, were observed. Attempts to stabilize this form by cooling a capillary containing it to the temperature of a dry ice trichloroethylene bath were unsuccessful.

### III. Identification of Dimethylberyllium

As shown above, this material was prepared by exactly the same method used by Gilman and Schulze (63). The physical properties, in regard to sublimation temperature and external appearance of the crystals,

were similar to those described by them. The purified crystals were dissolved in ether and tested for a metal-carbon linkage with Michler's ketone, according to the procedure of Gilman and Schulze (65). An immediate positive color test was obtained, in accordance with the results obtained by the authors cited. Since the reported physical properties are of a qualitative nature a rough chemical analysis was performed for the author by Mr. Ayres of the Institute for Atomic Research at Ames. A beryllium analysis performed on a small amount of sample gave a value of  $27 \pm 5\%$ . The theoretical value is 23.09%. The large limits of error are due to the small size of the sample used. Even at its widest limits this analysis is sufficiently accurate to eliminate the possibility of an etherate existing or of oxygen atoms being implicated in the structure. In addition, the experimental density of  $0.88 \pm 0.10$  g/cc. checks well with the X-ray density of 0.88 g/cc. As shall be shown, the symmetry of all possible space groups demand that all of the carbon atoms must be equivalent. The presence of methyl groups is shown by the fact that the hydrogen positions must be included in order to account for the intensities of low order reflections. Furthermore, the hydrogen electrons must be asymmetrically placed with respect to the carbon atoms which indicates that the methyl groups cannot be replaced by an atom of higher atomic number, such as nitrogen, which would have a symmetrical arrangement of electrons around the nucleus. The evidence listed above plus the excellent agreement of calculated and observed intensities comprise a sufficient proof of identity for this compound. In order to aid in future identification of dimethyl-

beryllium a list of d values and relative intensities is given in Table 5.

#### IV. Determination of the Structure

##### A. X-Ray Equipment

Diffraction data were obtained by means of Weissenberg, precession and powder cameras. The radius of the Weissenberg camera was 2.84 cm. The radius of the powder camera was 5.73 cm.

Weissenberg diagrams were obtained using filtered copper  $K\alpha$  radiation and filtered and unfiltered molybdenum  $K\alpha$  radiation. Precession diagrams were obtained using filtered and unfiltered molybdenum  $K\alpha$  radiation.

##### B. Measurement of Intensities

Intensities of Weissenberg reflections were estimated by the multiple film technique using five films. The factor between successive films for copper  $K\alpha$  radiation was assumed to be 3.7 for the Eastman Kodak No-Screen Medical X-ray film which was used for all exposures. Some precession diagram intensities were also estimated by the multiple film technique. Silver foil was placed between these films to increase the absorption of the molybdenum radiation, leading to a combined absorber-film factor of 5.3. Some intensities on precession diagrams were estimated by means of a series of timed exposures with a ratio of two between successive exposures. For zones where only single films were

Powder Diagram Intensities and d Values of Be(CH<sub>3</sub>)<sub>2</sub>

Table 5

Intensities	d	Indices
526	5.77	(020)
1000	5.42	(110)
73	3.07	(200)
700	2.96	(121)
73	2.88	(040)
176	2.42	(211)
110	2.21	(171)
216	2.10	(270)
	2.09	(002)
	2.08	(231)
16	2.01	(310)
11	1.92	(060)
20	1.81	(330)
30	1.76	(132)
30	1.73	(202)
65	1.69	(251)
	1.68	(161)
29	1.65	(222)
27	1.63	(260)
27	1.53	(400)
	1.53	(350)
37	1.50	(152)
52	1.45	(312)
	1.44	(080)
21	1.43	(411)
	1.41	(062)

available, intensities were determined by comparison with a series of films whose intensities had been determined by the multiple film technique.

Intensity data for the  $(hk0)$ ,  $(hkl)$ ,  $(h0l)$ ,  $(0kl)$ ,  $(1kl)$ ,  $(3kl)$ , and  $(hhl)$  zones were obtained on Weissenberg, rotation, and precession diagrams.

### C. Laue Symmetry

All Weissenberg and precession diagrams obtained around the three major perpendicular axes showed the symmetry  $C2l$ . The Laue symmetry is, therefore,  $D2h$  which is the orthorhombic diffraction symmetry.

### D. Determination of Lattice Constants

The lattice constants determined from  $hk0$  and  $0kl$  precession diagrams for the orthorhombic unit cell are

$$a_0 = 6.14 \pm 0.01 \text{ \AA.}$$

$$b_0 = 11.53 \pm 0.01 \text{ \AA.}$$

$$c_0 = 4.18 \pm 0.02 \text{ \AA.}$$

### E. Determination of the Density of Dimethylberyllium

The density of dimethylberyllium was determined by flotation comparisons in a series of liquids. The crystals were heavier than Skelly A ( $\rho = 0.4 \text{ g/cc}$ ) and cyclohexane ( $\rho = 0.78 \text{ g/cc}$ ) and were lighter than chlorocyclohexane ( $\rho = 0.98$ ) and chlorobenzene ( $\rho = 1.11 \text{ g/cc}$ ). The calculated densities for two, four, and six Be  $(\text{CH}_3)_2$  units per

cell are 0.44, 0.88, and 1.32 g/cc, respectively. Since this compound is body-centered the number of  $\text{Be}(\text{CH}_3)_2$  units per cell must be a multiple of two. Comparison of calculated values with the experimental range leads to four  $\text{Be}(\text{CH}_3)_2$  units per cell.

F. Determination of the Possible Space Groups

The Miller indices of all reflections from dimethylberyllium can be represented by the following relationships.

Reflection	Condition for Appearance
$(hk\ell)$	$\ell + h + k = 2n$
$(hk0)$	$h + k = 2n$
$(0k\ell)$	$k = 2n, \quad \ell = 2n$
$(h0\ell)$	$h = 2n, \quad \ell = 2n$

The symbol  $n$  denotes any integer. The condition that, for all reflections, the sum of the indices must be even indicates body centering. The  $(0k\ell)$  and the  $(h0\ell)$  data indicate the presence of  $b$  and  $a$  glide planes, respectively. All observable  $(0k\ell)$  and  $(h0\ell)$  indices conforming to the requirements of a body-centered lattice are listed in Table 6.

The number of extinctions observed for odd indices makes it probable that the glide planes really are present and that the odd index extinctions are not merely accidental. On this basis the two most probable space groups are  $D_{2h}^{26}$ -Ibam and  $C_{2v}^{21}$ -Iba in the nomenclature of the Internationale Tabellen zur Bestimmung von Kristallstrukturen (31). The small number of reflections observed to be present is due to the

Table 6

Observable  $(h0\ell)$  and  $(0k\ell)$  Indices

$(h0\ell)$ Reflections		$(0k\ell)$ Reflections	
$h=2n; \ell=2n$	$h=2n+1; \ell=2n+1$	$h=2n; \ell=2n$	$h=2n+1; \ell=2n+1$
* (200)	(101)	* (020)	(011)
* (400)	(301)	* (040)	(031)
* (600)	(501)	* (060)	(051)
* (002)	(103)	* (080)	(051)
* (202)	(303)	* (0·10·0)	(071)
* (402)	(503)	* (0·12·0)	(091)
(602)	(105)	* (002)	(0·11·1)
* (004)		(022)	(013)
(204)		* (042)	(033)
		* (062)	(053)
		(080)	(015)
		(0·10·2)	
		* (004)	
		* (024)	
		(044)	
		* (064)	
		(084)	

\* This symbol indicates observed reflections.



smallness of the lattice constants in the  $a_0$  and  $c_0$  directions and also to the large temperature factor which greatly weakens reflections of  $h$  or  $k$  index which are of large magnitude compared to the  $l$  index. The temperature factor will be discussed in detail in a later section. If one of the glide planes is not present the two most probable space groups are  $D_{2h}^{28}$ - $I$ mma and  $C_{2v}^{22}$ - $I$ ma. Calculations made on the basis of the  $b$  glide is not present in the space group  $D_{2h}^{28}$ - $I$ mma showed that, for this assumption, this space group is eliminated since no possible parameter values could account for the unobserved  $(h0l)$  reflections where the individual indices are odd.

#### G. Determination of Parameters

The intensity,  $I$ , of a reflection from a given plane of Miller indices,  $(hkl)$ , may be represented as follows

$$I = KFF^*LPAMT$$

Here  $F$  is the structure factor, which will be defined in the next equation.  $F^*$  is the complex conjugate of  $F$ .  $K$  contains universal constants plus the intensity of the incident beam, the exposure time, and factors dependent on the size of the crystal irradiated. These factors enter into  $K$  in such a manner that the intensities of reflections from the same zone measured on films exposed under different conditions are directly proportional to each other.  $L$  is the Lorentz factor which takes into account the varying times different planes are in position to give a reflection.  $P$  is the polarization factor which

corrects for the fact that a polarized source of X-rays is assumed in the derivation of  $K$ , whereas the incident beam is actually unpolarised.  $A$  is the absorption factor which takes into account absorption of X-rays by the crystal.  $M$  is the multiplicity factor which counts the number of equivalent planes which contribute to the same reflection.

Table 7

Possible Atomic Positions for  $\text{Be}(\text{CH}_3)_2$

Space Group	Positions
$C_{2v}^{21}$ -Iba	4: (a) $00z$ ; $0,0,1/2 + z$ 8: (c) $xyz$ ; $\bar{x}\bar{y}z$ ; $x,\bar{y},1/2 + z$ ; $\bar{x},y,1/2 + z$
$D_{2h}^{26}$ -Ibam	4: (a) $0,0,1/4$ ; $0,0,3/4$ 8: (j) $xy0$ ; $\bar{x}\bar{y}0$ ; $x, \bar{y},1/2$ ; $\bar{x},y,1/2$ Add (000) and $(1/2,1/2,1/2)$ to each position.

$T$  is the temperature factor which takes into account attenuation in the intensities of reflections caused by vibrations of the atoms.

$$F_{hkl} = f_1 \exp 2\pi i(hx_1 + ky_j + lz_k)$$

In this equation  $f_1$  is the atomic scattering factor which represents the ratio of the amplitude of the incident beam scattered by an atom to that scattered by an electron. The symbols,  $x_1$ ,  $y_j$ , and  $z_k$ , are the parameter values for each atom and locate the positions of the atoms in the unit cell in terms of the fraction of a translation along the three major axes of the cell.

The only space groups that will be considered are  $C_{2v}^{21}$ -Iba and  $D_{2h}^{26}$ -Ibam. Possible atomic positions are listed in Table 7. The other possible four-fold positions available in both space groups are equivalent to those listed since they do not change the relative positions of the beryllium and carbon atoms but merely involve a change in the origin of the unit cell. The other eight-fold positions in  $D_{2h}^{26}$ -Ibam are impossible because they do not allow any reflections to appear with odd index and many of these are observed.

In  $C_{2v}^{21}$ -Iba the square of the structure factor,  $FF^*$ , is equal to

$$FF^* = 16(f_{Be}^2 + 2f_{Be}f_C \cos 2\pi \ell z + f_C^2)$$

Since (008) is observed to be much of greater intensity than (006) the  $z$  parameter is restricted to regions around  $\frac{1}{4}$ . By noting at what value of the parameter,  $z$ , the intensity of (006) will equal that of (008) one can set safe limits on the  $z$  parameter. This procedure gives the value;  $z = 0.25 \pm 0.03$ . In space group  $D_{2h}^{26}$ -Ibam the structure factor for (00 $\ell$ ) data if  $z$  is equal to 0 is

$$F = 4f_{Be} + 8f_C$$

If  $z$  is equal to  $\frac{1}{4}$  the corresponding structure factor is

$$F = 4f_{Be} \cos 2\pi \ell / 4 + 8f_C$$

If the parameter is 0 one would expect a continuous normal decline of intensity at high orders due merely to the Lorentz and Polarization factors. For a parameter value of  $\frac{1}{4}$  there should be an alternation of intensities. Since there actually is an alternation of intensities the parameter in this space group must be  $\frac{1}{4}$ . The only difference

between the space groups is in the placement of the beryllium atoms with respect to the planes of carbon atoms. If the beryllium atoms are located exactly halfway between the planes containing the carbon atoms the space group is  $D_{2h}^{26}$ -Ibam. Any deviation from this position makes the space group  $C_{2v}^{21}$ -Iba. Since the z parameter is not distinguishable from  $\frac{1}{4}$  in the non-centrosymmetrical space group we shall consider it to have exactly this value and, therefore, in all of the discussion which follows shall consider only space group  $D_{2h}^{26}$ -Ibam.

Since the structure factors for (h00) and (0k0) reflections have exactly the same form, the values of the x and y parameters may be obtained in exactly the same manner. The form of the structure factors is given below.

$$F = 4f_{Be} + 8f_C \cos 2\pi hm \quad m = x \text{ or } y$$

Both of these equations contain just one unknown, the parameters themselves. By plotting calculated values of  $F^2$  against possible parameter values of x and y, respectively for various orders of (h00) and (0k0) and looking for regions on the plots where calculated ratios of  $F^2$  correspond with observed ratios one may obtain regions of possible parameter values. Observed values of  $F^2$  for (h00) and (0k0) reflections are listed in Table 8.

The condition,  $F^2(060) \geq F^2(080) < F^2(0 \cdot 10 \cdot 0)$ , leads to the following regions of parameter values for y.

0.096-0.102  
0.120-0.190  
0.398-0.404  
0.310-0.380

The condition that  $F^2(200) > F^2(400) < F^2(600)$  leads to the following regions of parameter values for  $x$ .

0.07-0.09  
 0.17-0.19  
 0.41-0.43  
 0.31-0.33

Table 8

Observed  $F^2$  Values for (h00) and (0k0) Data

Indices (h00)	$F^2$	Indices (0k0)	$F^2$
(200)	212	(020)	316
(400)	34	(040)	251
(600)	59	(060)	91
		(080)	85
		(0•10•0)	110

Ruling out duplications due to crystallographically identically sets the following parameter pairs are possible.

	x	y
A	0.07-0.09	0.096-0.102
B	0.07-0.09	0.398-0.404
C	0.07-0.09	0.310-0.380
D	0.07-0.09	0.120-0.190
E	0.17-0.19	0.096-0.102
F	0.17-0.19	0.120-0.190

G	0.17-0.19	0.398-0.404
H	0.17-0.19	0.310-0.380
I	0.41-0.43	0.096-0.102
J	0.41-0.43	0.120-0.190
K	0.31-0.33	0.096-0.102
L	0.31-0.33	0.120-0.190

The observation that (150) was not observed whereas (170) was present served to eliminate groups B, D, F, H, I, J, K, L. The condition that (220) is absent served to eliminate C, F, G, J, K. Comparison of (200) and (020) led to a strong reversal for set A. The condition that (022) is absent also eliminated set A. The only set which was possible was set E. The unrefined parameter values, therefore were

$$x = 0.17-0.19$$

$$y = 0.096-0.102$$

In addition to the trial-and-error method of determining approximate parameters described above, Patterson and Fourier projections of the structure were made in the xy plane. These projections led to parameters consistent with those determined by the trial-and-error method.

#### H. Temperature Factor and Parameter Refinement

On comparing  $F^2$ , calculated from the rough parameters with the observed  $F^2$  values it was evident that a large temperature factor correction was necessary since the calculated values at high indices were much larger than the observed ones. This correction is to be expected because of the lightness of the atoms in this compound and

also because of the type of bonding involved in the crystal. The bonding will be discussed in detail later.

The temperature factor has the form given below.

$$T = \exp(-2B \sin^2 \theta / \lambda^2)$$

The constant B was determined in the usual manner, from the slope of a plot of  $\log (F^2_{\text{observed}} / F^2_{\text{calculated}})$  versus  $\sin^2 \theta$  for (Ok0), (hk0), (hh0), and (h00) data, respectively. A value of B ( $5.88 \times 10^{-16}$ ) consistent with the slopes obtained on all of these plots was used. In determining the temperature factors the hydrogen positions described below were included in the calculation of  $F^2$ .

Application of this temperature factor to the (hk0) data gave good agreement at high orders, but the agreement was not as good as when this factor was used for (hk $\ell$ ) data. The larger the ratio of the  $\ell$  index to the h or k index the greater was the discrepancy between calculated and observed values. In addition, the value of B obtained from (00 $\ell$ ) data differed considerably from that obtained from (hk0) data. It was also noted on very intense films containing (h0 $\ell$ ) data that the (00 $\ell$ ) reflections extended to much higher angles than the (h00) or (h0 $\ell$ ) reflections. This evidence indicated the need for an anisotropic temperature factor. Since in this structure the extent of vibration in the  $a_0$  and  $b_0$  directions should be essentially the same, and since the same temperature factor satisfactorily accounted for all data in the {00 $\ell$ } zone, the temperature factors for all (hk0) data were assumed to be the same. The temperature factor constant B in the  $c_0$  direction was obtained from the (00 $\ell$ ) data. Its value is  $2.87 \times 10^{-16}$ .

The temperature factors were combined, in the standard manner (67), as shown below.

$$I_{\text{obs.}} = I_{\text{calc.}} \exp -(C \cos^2\theta + B) \sin^2\theta$$

Here  $C = A-B$  where  $A$  is the temperature factor in the  $c_0$  direction and  $B$  is the temperature factor in the  $\{001\}$  zone.  $\cos \theta$  is the direction cosine of a given plane.

A comparison of the application of the isotropic and anisotropic temperature factors is given in Table 9. In this calculation the

Table 9

Comparison of Isotropic and Anisotropic Temperature Factors

$hkl$	Number of Terms Considered	R isotropic	R anisotropic
$h1l$	8	0.14	0.10
$0kl$	11	0.13	0.09
$hhl$	8	0.22	0.09
$lkl$	16	0.17	0.16

refined parameters,  $x = 0.182$  and  $y = 0.101$ , were used and hydrogen positions were included. The function  $R$  is equal to

$$R = \frac{\sum_{hkl} ||F(hkl)_{\text{obs.}}| - |F(hkl)_{\text{calc.}}||}{\sum_{hkl} |F(hkl)_{\text{obs.}}|}$$

The relative values of  $R$  for a given set of data are a criterion of correlation. The smaller the value of  $R$  the better is the correlation between observed and calculated data. Because of the small number of reflections considered, the absolute value of  $R$  does not have much



significance. Only observed reflections were included in this calculation.

The anisotropic temperature factor gives a definitely better correlation factor in three of the four examples considered. There is not any significant difference in application of either method to  $(1k\ell)$  data. These data are the poorest quality of all of the zones listed since they were determined from a single film whereas the intensities of the other zones listed were determined from multiple films.

The x and y parameters were refined by a trial-and error procedure by comparison of the following pairs of reflections.

(080) and (420)

(080) and (440)

(510) and (190)

(510) and (0 $\cdot$ 10 $\cdot$ 0)

Intensities of the reflections listed were determined on an  $(hk\ell)$  precession diagram from timed exposures with a factor of two between successive exposures. The parameters were determined by setting the measured intensity ratio as an upper limit and setting a lower limit by applying a temperature factor correction greater than that determined above for the  $\{001\}$  zone. The temperature factor used in these calculations was  $8.2 \times 10^{-16}$  which is sufficiently above the experimentally determined factor of  $5.88 \times 10^{-16}$  to be a perfectly safe limit. By use of the limits described, it was possible to eliminate regions in parameter space which could not possibly account for either limit. Proceed-

ing in this way the following parameters were obtained.

$$x = 0.182 \pm 0.002$$

$$y = 0.101 \pm 0.002$$

### I. Effect of the Hydrogen Atoms

Hydrogen atoms might be expected to make a significant contribution to the intensities of low order reflections because of the comparative lightness of the other atoms as compared to hydrogen and also because of the relatively large number of hydrogens in the unit cell. Investigation of the low order data showed several discrepancies which could be improved by inclusion of hydrogen contributions. The calculated intensity of (040) was much too low when compared to the intensities of (020) and (002). The intensity of (200) was too low when compared with that of (002). Another difficulty was that (130) which was not observed, even on films of very long exposure time, should have been observed if the hydrogen contributions are neglected. Various attempts were made to account for the effect of the hydrogens. One method was to use the atomic scattering factor of fluorine for the methyl group. This procedure has the effect of placing all of the hydrogen electrons on the nucleus of the carbon atom. It cannot be strictly correct since the fluorine nucleus has a charge greater than that of the carbon atom and, therefore, the electrons will be too close to the nucleus. Another method was to approximate the atomic scattering factor of the methyl group by adding the difference between the scattering factors for unionized nitrogen and triply negatively

ionized nitrogen to the atomic scattering factor of carbon. The value of the methyl scattering factor was also calculated by the method of James and Brindley (66) using a carbon atom with three extra electrons in the p shell. This should be the most accurate method of approximation for a symmetrical arrangement of hydrogen electrons around carbon. None of these approximations helped to remove all of the discrepancies in the low order data. The most successful of these was the fluorine approximation which helped to raise the value of (040) but did not help regarding difficulties with (130) and (200). Mulliken (52) had suggested that in an electron-deficient compound, such as dimethylberyllium, the carbon atom uses its tetrahedral orbitals to bond the hydrogens. Accordingly the hydrogen atoms were tetrahedrally located with respect to the carbon atoms. The hydrogens were placed in the 16 and 8 fold positions of the space group  $D_{2h}^{26}$ -Ibam whose positions are listed below.

8: (j)  $xy0; \bar{x}\bar{y}0; xy\frac{1}{2}; \bar{x}\bar{y}\frac{1}{2} + (000); (\frac{1}{2}\frac{1}{2}\frac{1}{2})$

16: (k)  $xyz; \bar{x}\bar{y}\bar{z}; \bar{x}yz; xy\bar{z}; \bar{x},y,\frac{1}{2}+z; x,\bar{y},\frac{1}{2}-z; x,\bar{y},\frac{1}{2}+z; \bar{x},y,\frac{1}{2}-z$   
 $+ (000); (\frac{1}{2}\frac{1}{2}\frac{1}{2})$

Since there are two similar orientations of hydrogen atoms rotated at  $180^\circ$  with respect to each other, both sets of positions were used with half a hydrogen atom in each position. For the first trial the C-H distance was taken as 1.09 A., with the hydrogen parameters listed below.

	x	y	x	y
8 fold	0.349	0.068	0.125	0.187
16 fold	0.148	0.149	0.277	0.080

This procedure helped the low order intensity agreement somewhat but (040) was still too weak compared to (020) and the reversal between (200) and (002) remained. The intensity of (130) was reduced by a factor of two. It was found that the intensity agreement could be improved by shortening the C-H distance. Accordingly this distance was taken as 0.5 Å with the parameters listed below.

	x	y	x	y
8 fold	0.260	0.093	0.165	0.144
16 fold	0.167	0.126	0.227	0.094

Now the agreement in relative intensities of (020), (040), (200), and (130) was much improved. Although this procedure could have been continued, the use of 0.5 as the C-H distance gave satisfactory enough agreement between calculated and observed intensities that further refinement of the hydrogen parameters seemed unwarranted. This treatment does not really locate the hydrogen atoms, but it does show that their contributions cannot be neglected.

Including the hydrogen positions introduces complications in regard to the temperature factor correction. Although it might not be too bad an approximation to use the same temperature factor for both carbon and beryllium, yet the hydrogen atom must vibrate far more than the relatively heavy beryllium and carbon atoms. Although one should correct the hydrogen atomic scattering factors individually, this was not done, since it was deemed inadvisable in view of the other uncertainties involved. The hydrogen contribution, therefore, is probably weighted a little too heavily in the calculated intensities of the

higher order reflections. If the hydrogen contributions are included and if the x and y parameters are determined in the same manner as described before the following values are obtained. These values are identical to those obtained without inclusion of the hydrogen contributions.

$$x = 0.182 \pm 0.002$$

$$y = 0.101 \pm 0.002$$

#### J. Structure Factor Agreement

Calculated and observed structure factors are listed in Table 10. The observed values were corrected for Lorentz and polarization factors and the calculated values have been corrected by the anisotropic temperature factor described in section H. Intensities of reflections whose indices are not designated by reference to the footnotes of the table were obtained from  $(0k\ell)$ ,  $(1k\ell)$ ,  $(2k\ell)$ , and  $(3k\ell)$  precession diagrams. Intensities of  $(0k\ell)$  reflections were estimated from multiple films. Only single films were available for  $(1k\ell)$ ,  $(2k\ell)$ , and  $(3k\ell)$  reflections. Intensities on these films were estimated by comparison with both  $(hh\ell)$  and  $(0k\ell)$  multiple films. The average of the two measurements was taken for the measured intensity. Reflections designated in the footnotes as unobserved were unobserved because no data of a type that would include these reflections were obtained. The intensity estimation of observable reflections which are of high h or k index relative to the  $\ell$  index is not too accurate, since the high temperature factor in the  $\{001\}$  zone may reduce these intensities

Table 10

Observed and Calculated Structure Factors for Dimethylberyllium

Indices	Observed F	Calculated F
(020)	316	316
(040)	251	-264
(002)	182	198
(022)	0	-4
(060)	91	-91
(042)	167	216
(080)	85	86
(062)	142	-137
(082)	0	0
(0·10·0)	110	89
(004)	147	123
(024)	53	58
(110) <sup>abc</sup>	338	338
(130) <sup>c</sup>	0	20
(121) <sup>d</sup>		
(141)	127	-127
(112)	0	-5
(150)	0	-28
(132)	90	-90
(161)	69	89
(170)	46	40
(152)	97	-95
(181)	79	79
(123)	76	-106
(190)	59	58

- a (hh $\ell$ ) data
- b (h1 $\ell$ ) data
- c (hk0) data
- d (hkl) data
- e (h0 $\ell$ ) data

Table 10

(Continued)

Indices	Observed F	Calculated F
(172)	48	-56
(143)	51	-58
(163)	34	45
(1.10.1)	0	-4
(192)	0	-4
(114)	66	62
(1.11.0)	36	34
(134)	0	39
(183)	43	46
(154)	0	-1
(1.10.3)	0	2
(174)	34	13
(194)	46	22
(200) <sup>e</sup>	212	-212
(220) <sup>ac</sup>	0	9
(211) <sup>b</sup>	146	-140
(240) <sup>c</sup>	206	278
(202) <sup>e</sup>	163	-207
(251) <sup>d</sup>	27	17
(222) <sup>a</sup>	93	-93
(242) <sup>f</sup>		
(260) <sup>c</sup>	128	157
(271) <sup>b</sup>	68	73
(213)	36	-50
(280)	36	49
(262)	0	13
(233)	67	-68
(291)	0	22
(253)	0	0
(282)	39	-49

<sup>f</sup> Unobserved. For explanation refer to section J.

Table 10  
(Continued)

Indices	Observed F	Calculated F
(2·10·0)	0	-14
(273)	47	43
(204)	0	-9
(224)	0	15
(293)	0	20
(264)	55	43
(284)	0	0
(310) <sup>c</sup>	83	-102
(330) <sup>a</sup>	114	113
(321) <sup>d</sup>	36	19
(341) <sup>d</sup>	69	31
(350) <sup>c</sup>	187	162
(312) <sup>b</sup>	154	-145
(332) <sup>a</sup>	0	-2
(361) <sup>d</sup>	0	-16
(370) <sup>c</sup>	53	61
(381) <sup>d</sup>	0	-26
(323)	0	24
(372)	0	-11
(390)	0	-20
(343)	0	13
(363)	0	-10
(3·10·1)	0	0
(392)	55	-55
(3·11·0) <sup>c</sup>	0	-10
(314)	0	-9
(334)	31	36
(383)	0	0
(354)	58	54
(3·10·3)	0	0
(374)	0	22
(400) <sup>e</sup>	34	35
(420) <sup>e</sup>	54	43
(411) <sup>bd</sup>	72	68
(431) <sup>d</sup>	107	91



Table 10

(Continued)

Indices	Observed F	Calculated F
(440) <sup>a</sup>	37	43
(402) <sup>e</sup>	66	-44
(451) <sup>d</sup>	0	-2
(422) <sup>f</sup>		
(460) <sup>c</sup>	0	23
(471) <sup>d</sup>	88	-62
(480) <sup>c</sup>	0	17
(462) <sup>f</sup>		
(413) <sup>b</sup>	0	48
(491) <sup>d</sup>	0	20
(404) <sup>e</sup>	0	11
(424) <sup>f</sup>		
(444) <sup>a</sup>	0	10
(510) <sup>c</sup>	73	81
(530) <sup>c</sup>	0	12
(521) <sup>d</sup>	69	31

to a value so low that the reflections are unobservable. These reflections may actually have a finite intensity which, when corrected by the Lorentz and polarization factors, will bring their structure factors into closer agreement with the calculated ones.

The factor,  $R$ , described in section H is coming into increasing use as a criterion of correlation between calculated and observed structure factors. Its value for this structure, if only observed reflections are included is 0.13. Booth (68) has found that values of  $R$  ranging from 0.12 to 0.22 have been found for completed structures. The use of  $R$  as a criterion of reliability has been criticised, but a low value does indicate, in general, good agreement between calculated and observed intensities. The closeness of fit of the data is somewhat surprising when the errors in intensity determination are considered. One of the chief systematic errors in measuring intensities is the effect of absorption of X-rays by the glass capillaries which were employed. Inhomogeneities in capillary wall thickness will be reflected in errors in relative intensity measurement. Apparently the capillaries were thin enough that this was not as serious an error as might have been predicted. The effect of absorption in the crystals themselves was negligible due to the small size of the crystals employed and also because of the low scattering power of all of the components of this compound. No corrections for extinction were made.

#### K. Discussion of the Structure

The structure of dimethylberyllium consists of linear chains with

the beryllium and methyl groups in one chain arranged as shown in Figure 34. Two unit cells of the structure are shown in Figure 35. A view of the structure projected on the plane (001) is shown in Figure 36. A Fourier projection of the structure on (001) is shown in Figure 37. This structure is isomorphous with that of  $\text{SiS}_2$ . The Be-C distances in the electron-deficient bonds along the chains are  $1.93 \pm 0.02$  in the centrosymmetric space group, as compared with distances of 1.84 Å. calculated from Pauling's rule (69) and the following single bonded metallic radii;  $r_{\text{Be}} = 0.889$ ,  $r_{\text{C}} = 0.771$ . Pauling's rule is that interatomic distances may be calculated from the following equation, derived on empirical and theoretical grounds.

$$R(1) - R(n) = 0.300 \log n$$

$R(1)$  is the single bond radius;  $R(n)$  is the radius of an atom participating in a bond;  $n$  is the bond number, considered to be the number of electron pairs in the particular bond under consideration.

The C-Be-C angle in the four membered rings along the chain is  $114 \pm 1^\circ$ , in the centrosymmetric space group, which shows that there may be a slight distortion in this structure from the ideal tetrahedral angle of  $109^\circ 28'$ . Methyl-methyl distances between chains are 4.1 Å. which is perfectly normal for van der Waals distances between methyl groups. It may be seen in Figure 36, that the chains tend to pack in an arrangement very similar to the close packing of cylinders. If the chains really were closest packed, one could draw a hexagonal net which would pick out equivalent atoms in the (001) projection (Figure 36). The two dimensional unit cell of this net would have an obtuse angle

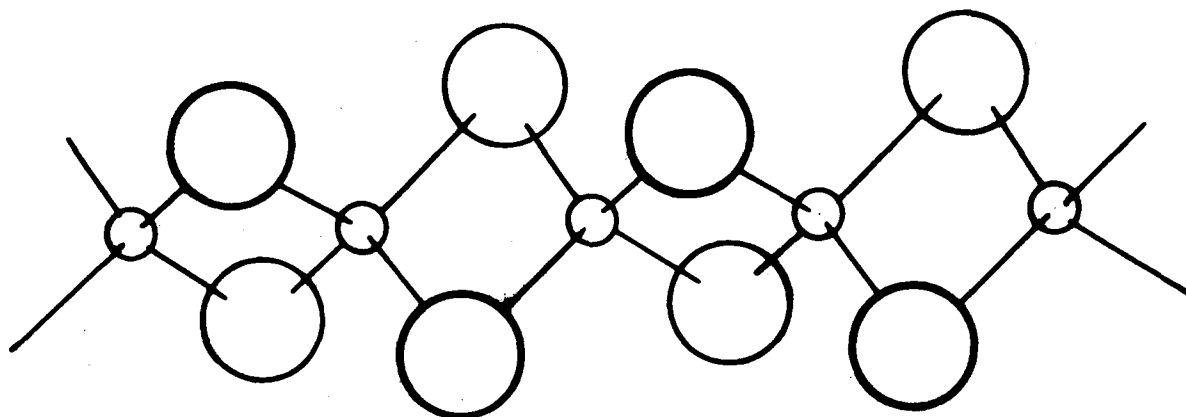


Fig. 34 - Arrangement of beryllium atoms and methyl groups in one continuous chain in the structure of dimethylberyllium. Large circles represent methyl groups. Small circles represent beryllium atoms.

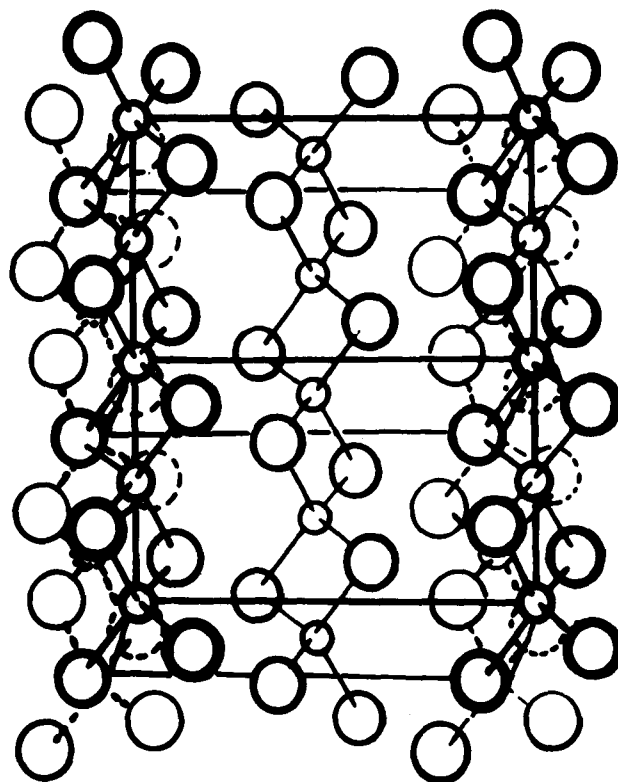


Fig. 35 - The structure of dimethylberyllium. Large circles represent methyl groups. Small circles represent beryllium atoms.

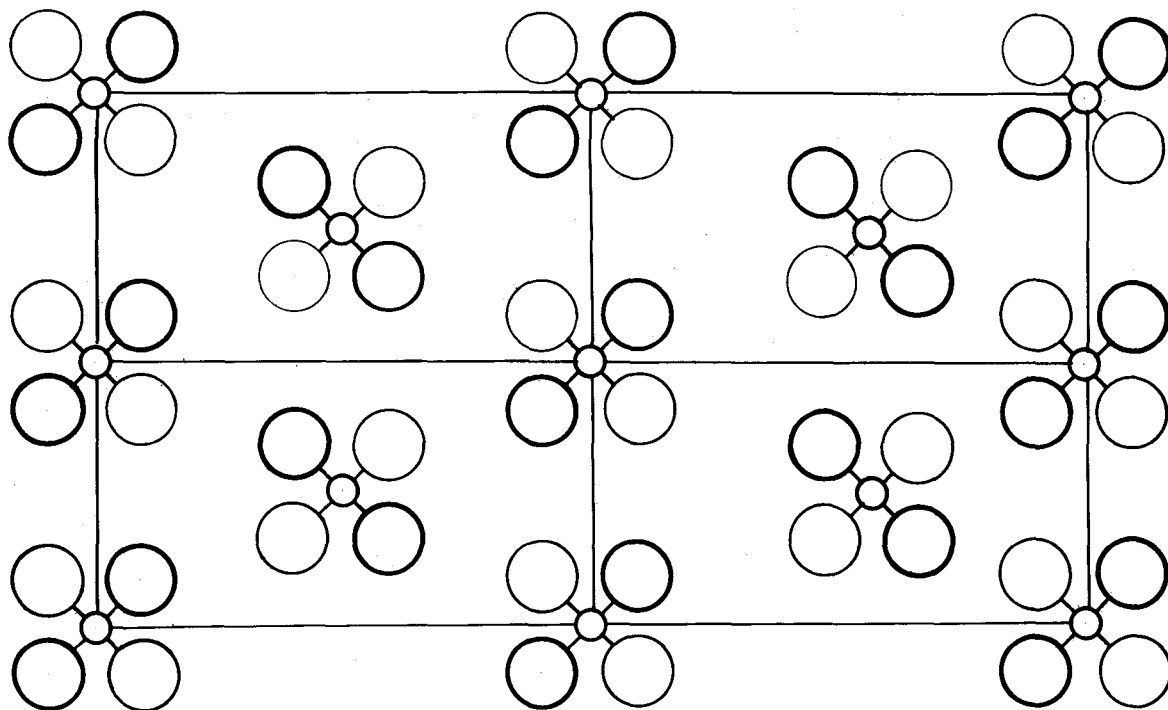


Fig. 36 - Projection of the structure of dimethylberyllium on (001).  
Large circles represent methyl groups. Small circles represent beryllium atoms.

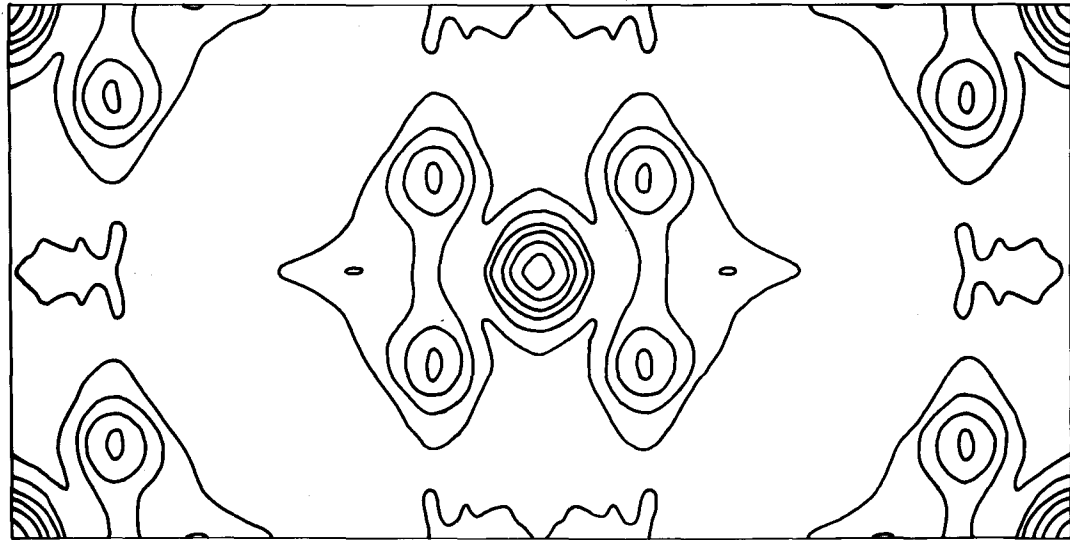
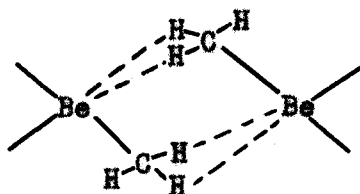


Fig. 37 - Fourier projection of dimethylberyllium on (001).

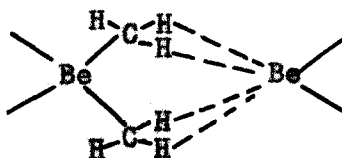
of  $120^\circ$ . If one draws an approximately similar net which would pick out equivalent atoms in the experimentally determined atomic positions, the obtuse angle of the two dimensional cell would now be  $124^\circ$ . Thus, there is a slight distortion from true closest packing.

The physical properties are compatible with the determined structure. The weak van der Waals forces between chains allow large vibration amplitudes perpendicular to the  $c_0$  axis, which accounts for the large temperature factor in these directions. The bonding along the chain is more rigid, which leads to a lower temperature factor in this direction. The bonding in the  $a_0$  and  $b_0$  directions is similar enough to account for the pronounced tendency of this compound to form twinned crystals along the fiber axis.

The configuration shown below, which is exactly analogous to the suggestion of Pitzer and Gutowsky (53) for trimethylaluminum, is prohibited by symmetry considerations alone.



An analogous type of structure is permitted by symmetry considerations.

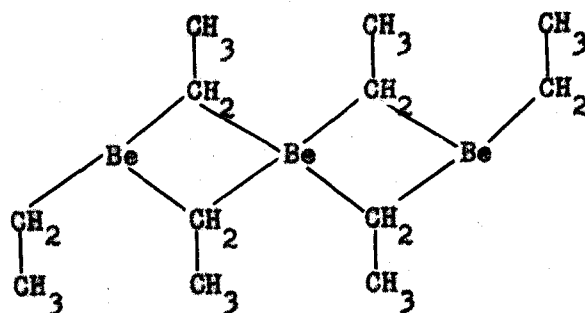


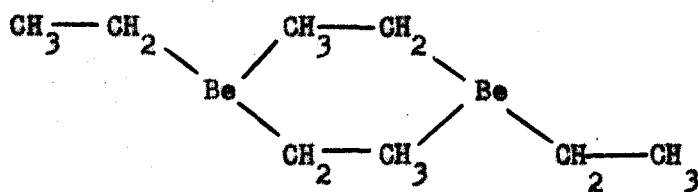


As shown in section G, however, the beryllium atom cannot be displaced from a location equidistant from the carbon atoms in the chain by more than 0.1 Å. This limit on displacement of the beryllium atoms makes the distance of the two shorter and two long bonds so nearly equal that this structure also is not permitted.

The geometry of the aluminum-methyl-aluminum bridge in trimethylaluminum has not yet been unambiguously determined. The compounds are similar enough that one would expect a type of bonding analogous to that of dimethylberyllium, with the aluminum atom in a symmetrical position between the four neighboring carbon atoms. This type of bonding has been previously suggested by Rundle (44).

In a recent investigation of diethylberyllium by Goubeau and Rodewald (70), the authors have suggested that it is a polymer. One evidence of polymerization is its high boiling point (180-240° C.) at atmospheric pressure as compared with diethyl zinc (118° C.) and diethyl mercury (159° C.). The Raman spectra are also interpretable on the basis that this compound is a polymer. The authors were unable to determine from the Raman spectra whether the polymer contained four or six membered rings. The two possibilities are shown below.





In the light of the dimethylberyllium structure and also the theory of electron-deficient bonding, the four membered ring is the more probable.

Rundle (44) has suggested a hybridization of the carbon atoms to permit more electron density in the bridge bonds than one electron pair. The geometry of the bridge bond with the sharp Be-C-Be angle of  $65\frac{1}{2}^{\circ}$  suggests that the methyl group remains essentially normal. The bonding is consistent with the suggestion of Mulliken (52) that one tetrahedral orbital of carbon is shared between beryllium orbitals to form one bonding orbital for the three atoms.

The Be-Be distance (2.09 A.) is short enough to suggest that there is some possibility of Be-Be bonding. This distance, however, is almost exactly the distance required by the essentially tetrahedral angle about beryllium and the required Be-C bridge distances. Pauling and Schomaker (78) have suggested that in bridge bonds of this type the metal has a coordination number which is greater than the number of low energy orbitals. Neither dimethylberyllium nor diborane are very good examples on which to check this theory, since in both compounds the small metal-metal distance is required by the metal-non-metal distances and angles. A better example is tetramethylplatinum in which the Pt-Pt distance is so long (54) that there are no good metal-metal bonds so that the metal is held together by entirely by electron-deficient bonding.

The determination of this structure extends the region of the periodic table where metal atoms are known to form electron-deficient compounds of the type considered here. Strictly metallic structures have been excluded from consideration. Tetramethyl platinum extended the known electron-deficient compounds to the eighth group and dimethylberyllium extends it to the second group of the periodic table. The only suggestion in accord with electron-deficient bonding in all known cases is the one first suggested by Rundle (56) that such bonding results from the tendency of a metal to use all of its low energy orbitals in bond formation even when these exceed the number of valence electrons.

### METALLIC VALENCES

The concept of valence has played a very important part in correlating and predicting the formulae and reactions of inorganic and organic compounds. Only recently, however, have attempts been made to apply valence concepts to intermetallic systems, both solid solutions and compounds. A pioneer in the field of application of valence concepts to metals is Hume-Rothery (71,72) who has made many correlations between analogous metal systems based on the concept that their properties depend to a great extent on the ratio of electrons to atoms. Perhaps the best known of these applications is to intermetallic compounds. He pointed out that certain intermetallic compounds with closely related structures, but unrelated stoichiometric composition, can be considered to have the same ratio of electrons to atoms. For compounds having the  $\beta$  brass structure the electron-to-atom ratio is  $3/2$ . For the  $\gamma$  brass structure the ratio is  $21/13$ . For the  $\epsilon$  brass structure the electron-to-atom ratio is  $7/4$ . These compounds do not have an absolutely fixed stoichiometric composition but actually have a solubility range which usually includes the electron-atom-ratios given above. Similarly, the principle of constancy of electron-to-atom ratio has been applied to correlate the solubility limits of various intermetallic solid solutions. In calculating the electron-to-atom ratio, he has, except for the transition metals, used valences suggested by chemical valences. Some typical valences used are given below.

Metal	Valence
copper	1
zinc	2
aluminum	3
silicon	4

A different procedure was followed in regard to transition metal valences. In order to obtain the same electron-to-atom ratios for compounds containing transition metals as for isomorphous compounds of known electron-to-atom ratio, he has assumed that the valences of transition metals are zero. Mott and Jones (73) have interpreted the zero valence obtained in this manner, as indicating that the transition metals contribute no bonding electrons to these compounds. Mott and Jones have assumed that in the transition metals, themselves, it is the unpaired electrons which are the bonding electrons. On this basis, one would expect 0.61 bonding electrons for nickel, 1.71 for cobalt, and so on, where these numbers correspond to the number of unpaired electrons in the element as determined from magnetic susceptibility data.

Pauling (69,74) has adopted a different approach to the concept of the valence of metals. The valences which he obtains differ from those used by Hume-Rothery for the transition metals, rare earths, and the families of the periodic table headed by copper, zinc, gallium, and germanium. For the remainder of the periodic table he used the same valences as Hume-Rothery. Pauling's transition metal valences were

derived from magnetic moment data in the following manner. The atomic saturation magnetic moment at absolute zero for iron is 2.22 Bohr magnetons indicating that there are 2.22 unpaired electrons in the metal. Pauling assumed that the remaining 5.78 electrons outside the argon-like core were bonding electrons. The constancy of the value, 5.78 was shown by the fact that there is an equal change in the value of average atomic number and saturation magnetic moment for iron and the elements immediately preceding and following it in the periodic table. When the average atomic number is greater than  $18 + 8.44$  the saturation magnetic moment begins to decrease at the same rate as it has increased in going from chromium to iron. Pauling assumed, therefore, that there are 2.44 non-bonding orbitals and that the decrease in saturation magnetic moment for alloys of average atomic number greater than 26.44 was due to the pairing of electrons in this non-bonding orbital. At an average atomic number between nickel and copper the magnetic moment is zero. Pauling assumed that at this point the non-bonding orbitals were filled with electrons. The extra electrons tend to decrease the valence of elements following nickel. Copper uses 2.44 electrons to completely fill the non-bonding orbitals with electron pairs. This leaves copper with 0.39 electron more than nickel outside the non-bonding orbitals. Because the interatomic distances in copper are greater than those of nickel Pauling assumed that the 0.39 electron paired with some of the bonding electrons, leading to a valence of 5.44

The essential difference between the Pauling and Mott and Jones points of view is that Mott and Jones regard the unpaired electrons as the bonding electrons, whereas Pauling regards these electrons as non-bonding electrons.

Methods of choosing between the two valence sets are not plentiful since, in general, they give results which are very close to each other. Jones (73) and Ewing and Pauling (75) have investigated the extent of filling of Brillouin zones in gamma brass. Using valences similar to those of Hume-Rothery, Jones considered the first zone to be bounded by the forms  $\{300\}$  and  $\{400\}$ . Using Pauling's valences, Ewing and Pauling considered the Brillouin zone bounded by the forms  $\{600\}$  and  $\{440\}$ . Since Pauling's valences are larger than those of Hume-Rothery for copper and zinc, he needs a larger zone to contain the electrons. Jones filled 93.5% of his zone and Ewing and Pauling filled 98.5% of their zone. On the basis of these data, Pauling's valences seem the better, if one grants that the complete filling of a zone leads to the lowest energy for a compound. There is a school of thought which holds that if the electrons fill the volume of a sphere inscribed in the zone and tangent to the zone boundaries then the lowest energy state is reached. On this basis Hume-Rothery's valences would seem to be the better. In any event this method of approach is not helpful in deciding which set does the better job of correlation.

There are many other examples of where application of Pauling's valences leads to results just as consistent as does the application

of Hume-Rothery's valences. Raynor (76) has recently used only Hume-Rothery's valences to interpret the following data. It is known that compounds which have the  $MgCu_2$ ,  $MgNi_2$ , or  $MgZn_2$  structures can be transformed from one of these structures into one of the other structures by replacing some of the element that is not magnesium by a foreign metal. In order to help in the clarification of the discussion which follows, electron-to-atom ratios for these compounds and valences of all of the elements discussed are given below.

Compound	Hume-Rothery Ratio			Pauling Ratio		
$MgZn_2$	2.00			3.63		
$MgCu_2$	1.33			4.29		
$MgNi_2$	0.66			4.52		
Valences	Mg	Zn	Cu	Ni	Si	Co
Pauling Basis	2	4.44	5.44	5.78	4	5.78
Hume-Rothery Basis	2	2	1	0	4	0

If silicon replaces copper in  $MgCu_2$  the  $MgZn_2$  structure is obtained. If a polyvalent metal replaces nickel in  $MgNi_2$ , the  $MgCu_2$  structure is obtained. If cobalt is added to  $MgZn_2$  the  $MgCu_2$  structure is obtained. Using the Hume-Rothery valences, Raynor was able to explain all of these transformations by noting whether the added metal tends to raise or lower the electron-to-atom ratio. One obtains exactly the same predictions by use of Pauling's valences, as may be seen by reference to the table above.

Raynor (76) has assumed that electron-to-atom ratio is important



in aluminum-transition element compounds. In calculating electron-to-atom ratios no consistent results are obtained if one uses the customary Hume-Rothery valence of zero for the transition metal. Instead Raynor assumes that each aluminum atom contributes three electrons and that the transition metal absorbs enough electrons to complete the filling of its non-bonding orbitals. He obtained approximate constancy of electron-to-atom ratio by this method and suggested that absorption of electrons from the structure by a transition metal is very likely. Electron-to-atom ratios calculated on Raynor's basis and also using Pauling's valences are shown below for aluminum alloys where all of the compounds come into equilibrium with the primary solid solution.

	CrAl <sub>7</sub>	MnAl <sub>6</sub>	FeAl <sub>3</sub>	Co <sub>2</sub> Al <sub>9</sub>	NiAl <sub>3</sub>
Raynor Method	2.05	2.05	1.58	2.17	2.09
Pauling Valences	3.35	3.40	3.70	3.51	3.70

If one ignores the ratio in the iron compound the Raynor ratios form a consistent set. There is no a priori reason for ignoring the valences of the iron compound, however. If all ratios are included the sum of the deviations from the average for the set using Pauling's valences is less than that using Raynor's valences. Raynor claims support is given for his views by the isomorphy of Co<sub>2</sub>Al<sub>9</sub> and FeNiAl<sub>9</sub> since they each contain approximately the same number of unpaired electrons in non-bonding orbitals. On the basis of Pauling's valences these two compounds should be isomorphous since they have identical electron-to-atom ratios.

Hume Rothery (77) has attempted to decide between his and Pauling's valence ideas by investigating the effect of manganese, iron, and nickel of the  $\alpha/\beta$  brass equilibrium, assuming that the major factor influencing the ternary isothermal, solid-solubility boundaries is the electron-to-atom ratio. By comparison of predicted and experimental solubility curves for isothermal solubility as a function of added transition element, he finds that if the metallic valences of copper, zinc, and aluminum are 1, 2, and, 3 respectively then the valences of manganese, iron, and nickel are 2, 1, and 0.4-0.6 respectively.

Hume-Rothery states that,

whatever may be the validity of Pauling's views regarding the number of electrons responsible for cohesion in the crystals of the transition elements, these numbers are not the effective valences of the atoms as regards the  $\alpha/\beta$  equilibrium.

and

... the directions of the curves are quite different from those to be expected for elements of valency 5 or 6.

Hume-Rothery's conclusions are valid only if copper and zinc have valences of 1 and 2 respectively. If one chooses a valence of 5.44 for copper as suggested by Pauling (74), and 3 for aluminum, one obtains a valence of 4.22 for zinc from the 550° C.  $\alpha/\beta$  boundary in the copper-aluminum-zinc system. Using these values for zinc and copper, on examination of the ternary solubility curves given by Hume-Rothery (77), the following valences are obtained: iron 5.44; manganese 4.22; and nickel 5.93-6.17. Pauling's values (74) are zinc 4.44; iron 5.78; manganese 4.16 and 5.78; and nickel 5.78. Not too much reliance is

to be placed on the exactness of the valences obtained, but the calculation outlined above does show that Pauling's valences, if changed slightly, form a self-consistent set.

Using the valences quoted above, one obtains exactly the same theoretical solubility curves as does Hume-Rothery. Giving copper a valence of 5.44, nickel has the highest valence of the three transition metals considered, whereas manganese has the lowest valence, a result in opposite order to that obtained by assuming copper to be univalent.

The particular ternary alloys considered by Hume-Rothery in his paper do not offer a means of distinguishing between the two viewpoints on valence, since both yield identical isothermal solubility curves.

One method of distinguishing between the two valence sets is to consider a ternary solid solution in which two of the components have valences for which Hume-Rothery and Pauling give identical values. If the third element is one on whose valences the two views disagree, different isothermal ternary solubility curves will be predicted on the basis of the two views. By comparison of calculated and empirical solubility curves, one may distinguish between the two points of view.

Even if constancy of electron-to-atom ratio, on which the above argument depends, is a valid concept, one must, however, consider carefully the effects of electronegativity, relative atomic size, and the orbitals available for bond formation in all of the components of the solid solution.

Examples of possible ternary systems which may be investigated are aluminum-beryllium-nickel, aluminum-beryllium-iron, and aluminum-beryllium zinc. The components of all of these systems have atomic radii which do not differ greatly and the electronegativities should not be greatly different. The system containing nickel should be an especially good one to investigate since the predicted valences of nickel are so different (0.60 vs. 5.78). By measuring the paramagnetism of the alloys containing paramagnetic elements additional conclusions may be deduced about the bonding in these alloys. Correlations of relative valences with compressibility and hardness data may also be possible.

## SUMMARY

### I. The Uranium-Carbon System

A constitutional diagram of the Uranium-Carbon system has been constructed from metallographic, thermal, chemical, and X-ray data. Two compounds, UC (4.8 wt% carbon) and UC<sub>2</sub> (9.16 wt% carbon), have been identified. There is no evidence of solubility of uranium or of higher carbides in UC. UC is stable at room temperature. UC<sub>2</sub> is stable only at high temperature and partially decomposes into UC and C at lower temperatures. At high temperatures and at compositions in the vicinity of 7 wt% C there is a possibility that either a compound, U<sub>2</sub>C<sub>3</sub>, which dissolves UC and UC<sub>2</sub>, exists or that UC and UC<sub>2</sub> form a continuous solid solution which extends over a range of approximately 9 atomic per cent. Although the Widmanstätten type structure indicates that the postulated U<sub>2</sub>C<sub>3</sub> exists as one phase at high temperature, all attempts to retain this one phase structure by quenching have been unsuccessful. Results of other workers (30) indicate that at a composition corresponding to U<sub>2</sub>C<sub>3</sub> a compound with very narrow solubility limits and unstable at temperatures above 1600° C. can be produced in samples that have been cold or hot worked. It has been shown that this compound, stable only below 1600° C., is not the phase which has decomposed into two phases to give the Widmanstätten structure.

The solubility of carbon in liquid uranium up to 1800° C. is small (less than 0.60 wt%), but the solubility increases rapidly with temperature thereafter. The gamma-beta and beta-alpha uranium solid

transformations are not affected by the presence of carbon.

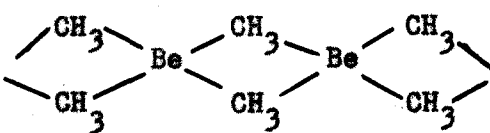
UC has a face centered cubic structure (NaCl type) with  $a_0 = 4.948 \pm 0.001$ .  $UC_2$  has a tetragonal structure ( $CaC_2$  type) with  $a_0 = 4.947 \pm 0.001$  and  $c_0 = 5.987 \pm 0.001$  A.

## II. The Structure of Dimethylberyllium

The proposal that metals with more low energy orbitals than valence electrons should form electron-deficient compounds when combined with groups with no unshared pairs has suggested that electron-deficient binding might occur in dimethylberyllium, a solid subliming at about  $200^\circ$  C.

Dimethylberyllium is orthorhombic with the following lattice constants:  $a_0 = 6.14$ ;  $b_0 = 11.53$ ;  $c_0 = 4.18$  A. It contains four  $Be(CH_3)_2$  units per unit cell. Weissenberg and precession data indicate the space groups  $D_{2h}^{26}$ -Ibam or  $C_{2v}^{21}$ -Iba.

Atomic positions were determined by trial and error methods and checked by Patterson and Fourier projections. The hydrogen atoms contribute significantly to the intensities of low order reflections.

The structure derived from X-ray data is isomorphous with that of  $SiSi_2$ . Continuous chains  with approximately tetrahedral configurations about beryllium are found in agreement with the fibrous nature of the crystals. The bond pair, Be-C-Be contains one electron pair. The observed Be-C distance is  $1.93 \pm 0.02$  A. for the centrosymmetric space group. The C-Be-C angle

in the ring is  $114 \pm 1^\circ$ . Methyl-methyl distances between chains are 4.1 Å which is normal for Van der Waals bonding, so that negative methyl ions are not indicated.

Space group  $C_{2v}^{21}-21$  would permit two short and two long bonds to beryllium, but intensity data restrict the difference to 0.1 Å, too symmetrical to allow structures similar to Pitzer and Gutowsky's proposal for trimethylaluminum, (53). It is suggested that the bonding in the trimethylaluminum dimer is similar to that in dimethylberyllium.

This is the first established electron-deficient bonding in the second group, the second outside the third group, and the second in which the methyl group is found bound to more than one other atom.

### III. Metallic Valences

Two different sets of valences are now being applied to metals in alloys, that of Hume-Rothery (71,72), Mott and Jones (73), and Pauling (69,74). In the former, metallic valences approach a minimum of or nearly zero for the transition metals, whereas in the latter a maximum of about 5.78 is reached for the same metals.

The applicability of both of these valence ideas to explanations of alloy solubility limits stoichiometric composition of intermetallic compounds, and the theory of metallic bonding has been discussed. In many of these applications the principle which has been used is that electron-to-atom ratio is an important factor in intermetallic interactions. It has been shown that for very many applications the Pauling

valences lead to exactly the same correlations and conclusions as do the Hume-Rothery, Mott and Jones valences.

A method of determining which valence set is the more applicable to explain intermetallic bonding has been proposed. Assuming constancy of electron-to-atom ratio is the governing factor in determining the isothermal solid solubility boundaries in ternary solutions, one may predict the slopes of the ternary solubility boundary curves if the valences of all of the components are known. By choosing ternary systems for which two of the components have valences for which Hume-Rothery and Pauling give identical values, one may find the valence the third element by comparing various predicted solubility boundary curves with the experimentally determined ones. Precautions which must be followed in this procedure and some possible ternary systems which fulfill the necessary conditions have been discussed.



LITERATURE CITED

1. Moissan, H., Compt. rend., 122, 247 (1896).
2. Lebeau, P., Compt. rend., 152, 955 (1911).
3. Ruff, O. and A. Heinzelmann, Z. anorg. u. allgem. chem., 72, 72 (1911).
4. Hagg, G. Z. physik. Chem., 12, 42 (1931).
5. Polushkin, E. P., Carnegie Schol. Mem., Iron Steel Inst. (London), 10, 137 (1920).
6. Battelle Memorial Institute, CT-541, Classified Report, Atomic Energy Commission, (Mar. 10, 1943).
7. Battelle Memorial Institute, CT-818, Classified Report, Atomic Energy Commission, (July 10, 1943).
8. Battelle Memorial Institute, CT-893, Classified Report, Atomic Energy Commission, (Aug. 10, 1943).
9. Carter, J. H. and A. I. Snow, CT-542, Classified Report, Atomic Energy Commission, (March 15, 1943).
10. Carter, J. H., CT-490, Classified Report, Atomic Energy Commission, (February 20, 1943).
11. Carter, J. H., A. H. Daane, and A. I. Snow, CT-751, Classified Report, Atomic Energy Commission, (June 24, 1943).
12. Warf, J. C., A. S. Newton, T. Butler, I. B. Johns and J. A. Ayres, CT-580, Classified Report, Atomic Energy Commission, (April 15, 1943).
13. Wilhelm, H. A. and A. H. Daane, CC-238, Classified Report, Atomic Energy Commission, (Aug. 15, 1942).
14. Carter, J. H., CT-1062, Classified Report, Atomic Energy Commission, (November 9, 1943).
15. Carter, J. H. and A. I. Snow, CT-609, Classified Report, Atomic Energy Commission, (April 24, 1943).
16. Battelle Memorial Institute, CT-1477, Classified Report, Atomic Energy Commission, (Mar. 1, 1944).

17. Creutz, E., CT-375, Classified Report, Atomic Energy Commission, (December 14, 1942).
18. Carter, J. H., A. I. Snow, and A. Tevebaugh, CT-686, Classified Report, Atomic Energy Commission, (May 22, 1943).
19. Snow, A. I., CT-954, Classified Report, Atomic Energy Commission, (October 2, 1943).
20. Snow, A. I., CT-891, Classified Report, Atomic Energy Commission, (Aug. 21, 1943).
21. Snow, A. I., CT-1180 (A-1661), Classified Report, Atomic Energy Commission, (Dec. 27, 1943).
22. Snow, A. I., CT-816, Classified Report, Atomic Energy Commission, (July 24, 1943).
23. Snow, A. I., CT-1102, Classified Report, Atomic Energy Commission, (Nov. 28, 1943).
24. Chiotti, P. and A. H. Daane, Metallurgical Project Record, Vol. XIX B, Classified Publication, Atomic Energy Commission, (1945).
25. Rundle, R. E., CT-686, Classified Report, Atomic Energy Commission, (May 22, 1943).
26. Baenziger, N. C. and R. E. Rundle, CT-1984, Classified Report, Atomic Energy Commission, (Nov. 10, 1944).
27. Rundle, R. E., N. C. Baenziger, A. S. Wilson, and R. A. McDonald, CC-1984, Classified Report, Atomic Energy Commission, (Feb. 17, 1945).
28. Rundle, R. E., and A. S. Wilson, CT-751A, Classified Report, Atomic Energy Commission, (June 24, 1943).
29. Rundle, R. E., N. C. Baenziger and A. S. Wilson, Metallurgical Project Record, Vol. XI B, Classified Publication, Atomic Energy Commission, (1945).
30. Mallett, M. W., A. F. Gerds, and D. A. Vaughan, BMI-T-19, Classified Report, Atomic Energy Commission, (January 31, 1950).
31. "Internationale Tabellen zur Bestimmung von Kristallstrukturen", Rev. Ed., Gebruder Borntraeger, Berlin, 1935.
32. Wiberg, E., Ber., 69, 2816 (1936).

33. Dilthey, W., Z. angew. Chem., 34, 596 (1921).
34. Core, A. F., Chemistry and Industry, 5, 642 (1927).
35. Mark, H. and E. Pohland, Z. Krist., 62, 103 (1925).
36. Bauer, S. H., Chem. Rev., 25, 180 (1942).
37. Shand, W., Chem. Eng. News, 24, 2950 (1946).
38. Anderson, T. F. and A. B. Burg, J. Chem. Phys., 6, 586 (1938).
39. Bell, R. P., and H. C. Longuet-Higgins, Proc. Roy. Soc., 183 A, 357 (1945).
40. Price, W. C., J. Chem. Phys., 15, 614 (1947).
41. Nekrasov, V., J. Gen. Chem., (U.S.S.R.), 10, 1021 (1940).
42. Diatkina, M. E. and J. K. Sirkin, Compt. rend. acad. sci. U.R.S.S., 35, 180 (1942).
43. Pitzer, K. S., J. Am. Chem. Soc., 67, 1126 (1945).
44. Rundle, R. E., J. Am. Chem. Soc., 69, 2075 (1947).
45. Walsh, A. D., J. Chem. Soc., 89 (1947).
46. Burawoy, A., Nature, 155, 328 (1945).
47. Longuet-Higgins, H. C. and R. P. Bell, J. Chem. Soc., 250 (1943).
48. Sirkin, J. K., and M. E. Diatkina, Acta Physicochim. U.R.S.S., 14, 547 (1941).
49. Bell, R. P. and H. J. Emeleus, Quart. Rev., 2, 132 (1948).
50. Rundle, R. E., N. C. Baenziger, A. S. Wilson and R. A. McDonald, J. Am. Chem. Soc., 70, 99 (1948).
51. Webb, A. N., J. T. Neu and K. S. Pitzer, J. Chem. Phys., 17, 1007 (1949).
52. Mulliken, R. S., J. Chem. Phys., 3, 635 (1935).
53. Pitzer, K. and H. Gutowsky, J. Am. Chem. Soc., 68, 2204 (1946).
54. Rundle, R. E. and J. H. Sturdivant, J. Am. Chem. Soc., 69, 1561 (1947).

55. Rundle, R. E., Acta Cryst., 1, 180 (1948).
56. Rundle, R. E., J. Am. Chem. Soc., 69, 1327 (1947).
57. Rundle, R. E., J. Chem. Phys., 17, 671 (1949).
58. Stitt, F., J. Chem. Phys., 9, 780 (1941).
59. Stitt, F., J. Chem. Phys., 8, 981 (1940).
60. Burg, A., J. Am. Chem. Soc., 69, 747 (1947).
61. Seitz, F., "Modern Theory of Solids", McGraw-Hill Book Company, Inc., New York, 1940, p. 254-345.
62. Pauling, L., Physica., 15, 23 (1949).
63. Gilman, H., and F. Schulze, J. Chem. Soc., 2663 (1927).
64. Newton, A. S., MDDC-724, Declassified Report, Atomic Energy Commission, (January 1, 1947).
65. Gilman, H. and F. Schulze, J. Am. Chem. Soc., 49, 2907 (1925).
66. James, R. W. and G. W. Brindley, Phil. Mag., 12, 81 (1931).
67. Zachariasen, W. H., "Theory of X-Ray Diffraction in Crystals", John Wiley and Sons, Inc., New York, 1945, p. 208.
68. Booth, A. D., "Fourier Technique in X-Ray Structure Analysis", University Press, Cambridge, 1948, p. 101.
69. Pauling, L., J. Am. Chem. Soc., 69, 542 (1947).
70. Goubeau, J. and B. Rodewald, Z. anorg. Chem., 258, 162 (1949).
71. Hume-Rothery, W., "The Structure of Metals and Alloys", Institute of Metals, London, 1944.
72. Hume-Rothery, W., "Atomic Theory for Students of Metallurgy", Institute of Metals, London, 1946.
73. Mott, N. F. and H. Jones, "Theory of the Properties of Metals and Alloys", Clarendon Press, Oxford, 1936.
74. Pauling, L., Phys. Rev., 54, 899 (1938).
75. Ewing, F. J. and L. Pauling, Rev. Mod. Phys., 20, 112 (1948).
76. "Progress in Metal Physics", Intersciences Publishers, Inc., New York, 1949, p. 1-73.

77. Hume-Rothery, W., *Phil. Mag.*, 39, 89 (1948).
78. Pauling, L. and V. Schomaker, (Private Communication to Dr. R. E. Rundle), California Institute of Technology (1948).

#### ACKNOWLEDGMENTS

The author is deeply grateful to Dr. R. E. Rundle for suggestion of the dimethylberyllium problem and for his continued interest, guidance, and encouragement during the course of this investigation. The author is also indebted to Dr. Rundle for helpful discussion of the problem of metallic valences.

The author is indebted to Dr. H. A. Wilhelm for helpful discussion of the uranium-carbon system.

The author is also indebted to Dr. J. H. Carter with whom some of the early work on the uranium carbon system was performed and who taught the author a great deal concerning metallurgical techniques.

The author is also indebted to the following: to Mr. P. Chiotti for Figures 23, 24, 25, 26 and 29; to various members of the analytical section of the Ames Laboratory of the Atomic Energy Commission under the direction of Dr. J. C. Warf for some of the analyses in the uranium-carbon system.

The author is grateful to the Ames Laboratory of the Atomic Energy Commission for providing funds and facilities for the research presented in this paper.